NEUROIMMUNOLOGY

The meninges host a distinct compartment of regulatory T cells that preserves brain homeostasis

Miguel Marin-Rodero[1], Elisa Cintado[2], Alec J. Walker[3,4,5], Teshika Jayewickreme[1], Felipe A. Pinho-Ribeiro[1]†, Quentin Richardson[1], Ruaidhrí Jackson[1], Isaac M. Chiu[1], Christophe Benoist[1], Beth Stevens[3,4,5,6], José Luís Trejo[2], Diane Mathis[1]*

Our understanding of the meningeal immune system has recently burgeoned, particularly regarding how innate and adaptive effector cells are mobilized to meet brain challenges. However, information on how meningeal immunocytes guard brain homeostasis in healthy individuals remains limited. This study highlights the heterogeneous, polyfunctional regulatory T cell (T_{reg}) compartment in the meninges. A T_{reg} subtype specialized in controlling interferon-gamma (IFN-γ) responses and another dedicated to regulating follicular B cell responses were substantial components of this compartment. Accordingly, punctual T_{reg} ablation rapidly unleashed IFN-γ production by meningeal lymphocytes, unlocked access to the brain parenchyma, and altered meningeal B cell profiles. Distally, the hippocampus assumed a reactive state, with morphological and transcriptional changes in multiple glial cell types. Within the dentate gyrus, neural stem cells underwent more death and were blocked from further differentiation, which coincided with impairments in short-term spatial-reference memory. Thus, meningeal T_{regs} are a multifaceted safeguard of brain homeostasis at steady state.

INTRODUCTION

The meninges constitute a three-layered structure just under the skull and vertebral column, covering the brain and spinal cord. This brain border, in particular the dura mater layer, hosts a dense and highly diverse constellation of immunocytes at homeostasis (*1*, *2*) as well as a dedicated lymphatic drainage system (*3*). Many of these cells are members of the innate immune system, especially macrophages (MFs), but there are also small populations of lymphocytes whose functions are not well understood. For example, severe combined immunodeficiency patients and mice lacking T and B cells have behavioral abnormalities that resolve with reconstitution of the adaptive immune system (*4*–*7*). T cells seem especially important for brain homeostasis because the cytokines they produce impact various behavioral parameters as well as promote cognitive changes with aging (*8*–*17*).

Even less well-understood are the cellular regulators of meningeal immunocyte responses. Most types of immune reactions are controlled by Foxp3+CD4+ regulatory T cells (T_{regs}), which can restrain an immune response directly by acting as a sink for IL-2, by secreting suppressive factors like IL-10 or transforming growth factor–β (TGF-β), or by expressing co-inhibitory molecules such as CTLA-4, PD-1, or LAG-3 (*18*). In addition, they can act indirectly by modulating the differentiation and presentation capacity of antigen-presenting cells (APCs) such as dendritic cells (DCs) and MFs. T_{regs} in non-lymphoid tissues ("tissue-T_{regs}") also control non-immunological processes, notably promoting tissue repair, including in response to central nervous system (CNS) pathologies such as stroke or experimental autoimmune encephalomyelitis (EAE) (*19*).

The presence of T_{regs} in the meninges of old or diseased mice has been reported [e.g. (*20*)], but their function remains unclear. Here, we have addressed their role in promoting homeostasis of the brain meninges and parenchyma. Our work highlights a population of T_{regs} present in the meningeal dura mater of healthy mice, clustered with DCs along the sinuses. These T_{regs} restrain local interferon-gamma (IFN-γ) production and inflammation, and protect the brain's functional integrity at steady state by inhibiting immunocyte infiltration into the parenchyma and preserving neurogenesis within the hippocampal niche. Our findings both extend the purview of tissue-T_{regs} and bring to light an important immunological regulator of brain homeostasis.

RESULTS

The dural layer of the meninges hosts a distinct population of Foxp3$^+$CD4$^+$ T cells at steady state

Very little is known about the representation, phenotype, and function of meningeal T_{regs}, especially at steady state. Therefore, we performed a cytofluorometric analysis of the Foxp3$^+$CD4$^+$ compartment of meninges isolated from transcardially perfused, 6-week (wk)-old, male, C57BL/6 (B6) mice (Fig. S1A). We focused on the dura mater because the other meningeal layers contain far fewer immunocytes at steady state (*2*, *21*), and these layers take substantially longer to cleanly isolate. We could readily identify a population of Foxp3$^+$CD4$^+$ T cells in the meninges (Fig. 1A), fractionally slightly higher than in the spleen (Fig. S1B), greater than an order of magnitude more abundant than in the leptomeninges (>15x), and even more frequent than in the choroid plexus (>29x) (Fig.S1C, D). At an average of about 125 T_{regs} per mouse, the meningeal T_{reg} population was evident but small enough to limit the use of some experimental approaches to characterize them.

Confocal microscopy of tissue obtained from B6.*Foxp3*^{Gfp} mice provided an independent confirmation of the meningeal T_{reg}

[1]Department of Immunology, Harvard Medical School; Boston, MA, USA. [2]Cajal Institute, Translational Neuroscience Department, Consejo Superior de Investigaciones Científicas; Madrid, Spain. [3]F.M. Kirby Neurobiology Center, Boston Children's Hospital, Boston, MA, USA. [4]Harvard Medical School; Boston, MA, USA. [5]Stanley Center for Psychiatric Research, Broad Institute of MIT and Harvard; Cambridge, MA, USA. [6]Howard Hughes Medical Institute, Boston Children's Hospital; Boston, MA, USA.
*Correspondingauthor.Email: dm@hms.harvard.edu
†Present address: Division of Dermatology, John T. Milliken Department of Medicine, Washington University School of Medicine in St Louis, St Louis, MO, USA.

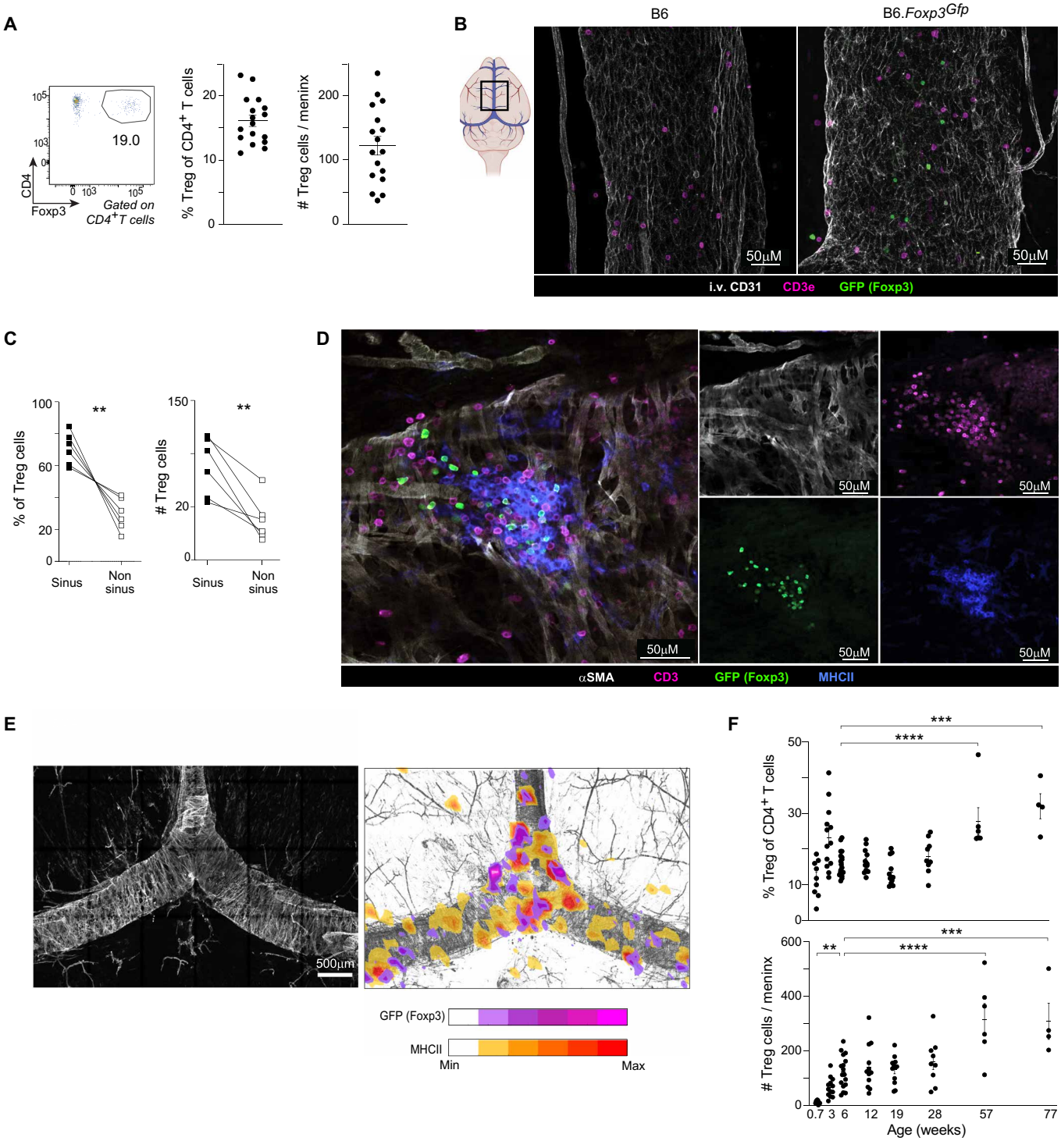

Fig. 1. A population of Foxp3$^+$CD4$^+$ T cells within the meningeal dura at steady state. (**A**) Flow cytometry of Foxp3$^+$CD4$^+$ T cells in the dural meninges of 6wk-old mice. Left panel: representative flow-cytometric plot; Right panels: summary data. n = 17. (**B**) Confocal imaging of transverse sections of the dura mater. Left panel: graphical representation of the meningeal sinuses, with the region of interest delineated by a square; right panels: representative images. (**C**) Representative confocal image of a meningeal T_{reg} cluster on a transverse section stained for the indicated marker proteins. (**D**) Quantification of T_{reg} locations. n = 6. (**E**) Tile-scan images of multiple duras registered to a reference map (left), plotting average densities of the Foxp3-GFP and MHC-II signals across 6 tissues (right). (**F**) Quantification of T_{regs} in the dura mater across age. n ≥ 4. Each data-point is from an individual mouse. iv, intravenous; SMA, smooth-muscle actin; MHC, major histocompatibility complex. Mean ± SEM. ∗p < 0.05, ∗∗p < 0.01, ∗∗∗p < 0.001, ****, p < 0.0001 by paired Student's *t* test [(C)] or one-way ANOVA [(F)]. Summary plots show data pooled from ≥2 independent experiments.

compartment. Most T_{regs} were close to the dural sinuses, accompanied by other types of T cells (Fig. 1B). While some T_{regs} were dispersed along the sinuses, they often formed clusters (Fig. 1C), especially with other T and major histocompatibility complex class II ($MHCII^+$) cells (Fig. 1D, E). The latter cells were mostly type 2 conventional DCs (cDC2s), defined as $MHCII^+CD11c^+F4/80^-Sirpa^+$ (*22*) (Fig. S1E, F). Clustering of T_{regs} and $MHCII^+$ cells within the dural sinuses was confirmed in multiple mice ranging from 5 to 16 wks of age (Fig. S2A, B). To gain a more comprehensive view of the dura mater, we registered tile-scan images of multiple duras to a reference map and then plotted the average density of GFP (Foxp3) and MHCII signals across all 6 tissues, which again highlighted T_{reg}:APC clustering (Fig. 1E).

Aging was associated with a decline in the total number of $CD45^+$ cells in the meninges (Fig. S2C). In contrast, the fraction and number of meningeal T_{regs} showed a general increase with age (Fig. 1F), consistent with a published comparison of 2- and 24-month-old mice (*20*). Total $CD45^+$ cells and T_{regs} accumulated in the meninges of male and female mice to a similar degree (Fig. S2D, E).

The meningeal T_{reg} compartment is a heterogeneous population with repeated TCR sequences

T_{regs} operating in non-lymphoid tissues have distinct transcriptomes, T cell receptor (TCR) repertoires, and growth-factor dependencies, enabling their functional adaptation and survival within particular settings (*19*). To explore their phenotype and functional potential, we performed population-level RNA sequencing (RNA-seq) on three meningeal-T_{reg} replicates, each pooled from five 15wk-old males. T_{regs} in meninges were distinct from those in lymphoid tissues and in all other non-lymphoid tissues, including inflamed brain (*23*) (Fig. S3A). Nonetheless, meningeal T_{regs} preferentially expressed a previously reported pan-tissue-T_{reg} signature (*19*) in comparison with their splenic counterparts (Fig. S3B). The meningeal-T_{reg} transcriptome was enriched in transcripts encoding molecules involved in cell adhesion and locomotion (e.g. *Ccl5*, *Cxcl10*, *Itga4*, *Itgav*, *Ccr2*, *Cxcr3*); promotion of cell death; the inflammatory response; regulation of myeloid-cell differentiation; and, notably, regulation of neuron death (*Ifng*, *Il10*, *Cd200r*, *Wisp*, *Ptgs1*) (*24*–*30*) (Fig. S3C). The transcriptomes of meningeal T_{regs} from male and female mice were very similar, the major difference being an enrichment for cell-cycle pathways in males (Fig. S3D, E), a finding confirmed by their higher fraction of $Ki67^+$ cells (Fig. S3F). Similarly, an elevation in cell-cycle pathways was the major transcriptional feature distinguishing adult (16wk-old) from old (53wk-old) mice (Fig. S3G, H).

Skull bone marrow (BM) and the meninges are interconnected by small conduits through which myeloid and B cells are able to migrate (*31*–*33*). Although T cells have been reported to access the meninges via the circulation (*32*, *34*), we compared the transcriptomes of T_{regs} isolated from the meninges and skull BM, in part to assess potential contamination of the meningeal-T_{reg} isolate by skull-BM cells. The two T_{reg} compartments were clearly distinct (Fig. S3J), the meningeal population expressing relatively few transcripts specifying molecules related to catabolic processes and protein transport and enriched in transcripts encoding proteins involved in metabolic pathways (Fig. S3I).

To explore the subtype heterogeneity of meningeal T_{regs}, we sorted the total $CD4^+$ T cell populations from two cohorts of mice (15 and 25 individual mice) and performed scRNA-seq coupled with sc*Tra/b*-seq. After quality control, we retained a total of 4090 $CD4^+$ T cells, with a mean of 2453 unique fragments per cell. Dimensionality reduction, unsupervised clustering, and signature overlay revealed a clear group of $Foxp3^+$ T_{regs} (Fig. S4A), which we extracted for downstream analyses. Re-clustering the T_{regs} revealed three distinguishable subtypes (Fig. 2A), each with approximately equal fractional contributions from the two scRNA-seq replicates (Fig. S4B). A heatmap of the most differentially expressed genes confirmed the cluster parsing (Fig. 2B), and the genes' identities prompted us to annotate the clusters "T helper (T_H)-1-like", "T follicular regulatory (T_{FR})-like", and "quiescent." T_H1-like T_{regs} express the transcription factor (TF) Tbet and multiple interferon-stimulated genes (ISGs), notably *Cxcr3*, and control T_H1, $CD8^+$ T, and NK cell responses (*35*, *36*). Tfr cells, expressing transcripts encoding CXCR5 and PD-1, are generally localized in follicles or germinal centers (GCs), where they control the magnitude and output of the local B cell response (*37*, *38*). The so-called quiescent cluster, typical of tissue-T_{regs}, expresses genes characteristic of unreactive T_{regs} (*39*, *40*). The three subtype designations were further reinforced by overlaying corresponding gene signatures (*19*, *39*, *41*, *42*) (Fig. 2C) or key marker transcripts (Fig. S4 C-E) on the UMAP. Lastly, flow cytometry confirmed the existence of the three subtypes within the meningeal T_{reg} compartment, each as a higher fraction of $CD4^+$ T cells than was found in the spleen (Fig. 2D-F). Also consistent with the T_{reg} subtype designations is that analogous processing of the non-T_{reg} $CD4^+$ T cells from the same scRNA-seq cohorts yielded clear T_H1, IFN-responsive, and T_{FR} clusters (Fig. S4F).

From the same two cell pools, we also obtained sc*Tra/b* sequences. We were particularly interested in repeat sequences, defined as the presence of two or more cells with the exact same nucleotide sequences encoding their TCRα and TCRβ chains, suggestive of clonality. Even though we could examine sequences from a total of only 366 cells from a total of 40 mice (data file S1), making detection of repeats rather unlikely, we observed 5.5% repeat sequences within the total dataset. Intra-subtype sharing was restricted to the T_H1-like cluster (Fig. 2G); in addition, a few repeat sequences were shared between the T_H1-like cluster and the T_{FR}-like or quiescent clusters (Fig. 2H, I).

Meningeal T_{regs} restrain the proliferation and IFN-γ production by local lymphocytes

To investigate their function in the meninges, we performed punctual T_{reg} depletion in 6wk-old B6.*Foxp3.Dtr*$^+$ and B6.*Foxp3.Dtr*$^-$ male littermates (hereafter referred to as DTR^+ and DTR^-, respectively) by intraperitoneal (ip) injection of diphtheria toxin (DT) on three consecutive days, followed by analysis 3 days after the last injection (Fig. 3A). This relatively short depletion protocol, chosen to minimize long-range systemic influences, effectively reduced the frequency of T_{regs} in the meninges (Fig. 3B) without affecting total immunocyte numbers (Fig. 3C). Nonetheless, the fractions and numbers of αβT and B cells increased and decreased, respectively, with no evident changes in the frequencies of other major immunocyte types (Fig. 3D). Meanwhile, splenic immunocyte and T cell numbers remained unchanged (Fig. S5A). Within the meningeal T cell population, both the $CD4^+$ and $CD8^+$ fractions expanded, while the double-negative fraction decreased (Fig. 3E). Confocal imaging of meninges whole-mounts revealed the expanded T-cell populations to be confined to the typical niche, accompanied by an increased MHCII signal (Fig. 3F). The B-cell loss reflected a reduction in the follicular B cell stages (Fig. 3G; Fig. S5B). Additionally, meningeal T_{regs} formed clusters in close proximity to B cells (Fig. 3H).

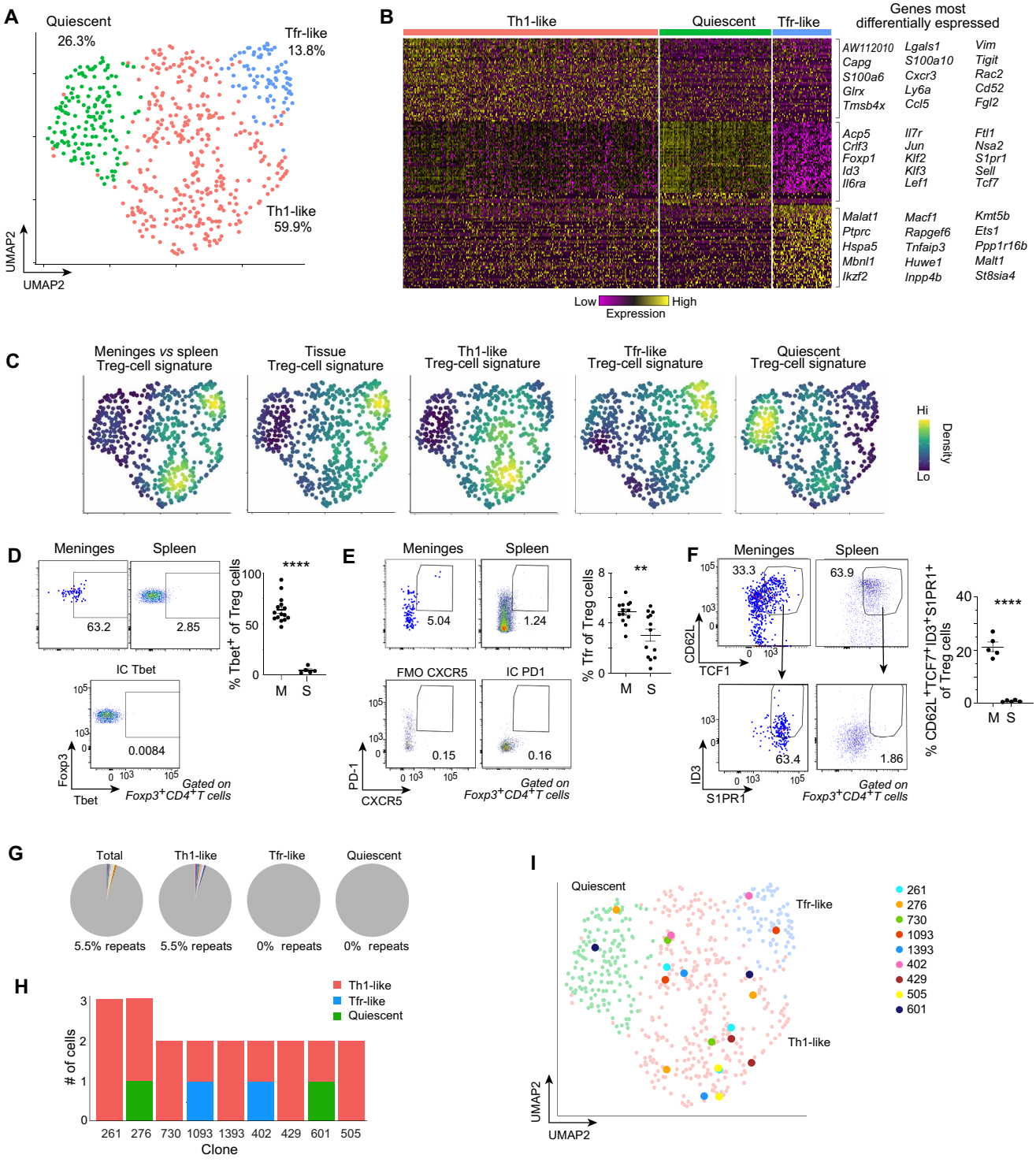

Fig. 2. Heterogeneity and clonal expansions within the meningeal T_{reg} compartment. (**A-C**) Merged scRNA-seq data from dura mater T_{regs} of 40 mice (15 weeks: n = 15, 36 weeks: n = 25). (A) UMAP plot. Percentages indicate the fractional representation of each cluster. (B) Heatmap of the 50 genes most differentially expressed by each cluster. The 10 genes (excluding *Rps* genes in cluster 2) most specific are indicated to the right. (C) Expression density plots of the indicated signatures. (**D-F**) Flow cytometry of the three meningeal T_{reg}-subtypes' key marker proteins. Left: representative dot plots; right: summary data. For (E) and (F) representative flow plots depict 3 samples concatenated. (**G-I**) sc*Tcr*-seq data from the meningeal T_{reg}-subtypes. (G) Pie-charts showing the proportion of clonally expanded cells in each cluster. Individual clones are depicted by different colors; non-expanded clones are in gray. (H) Bar plot showing the clonal overlap between the various clusters. x-axis: clone names: y-axis: number of T_{regs} of that particular clone. Bar colors correspond to the clusters of (A). (I) Expanded TCR clones situated on the UMAP plot from (A). UMAP, Uniform Manifold Approximation and Projection; Tfr, T follicular regulatory cell; Th1, T helper1; M, meninges; S, spleen; IC, isotype control; FMO, fluorescence minus one. Mean ± SEM, p-values as per Fig. 1. Mean ± SEM; p-values as per Fig. 1 by unpaired Student's *t* test [(D-F)]. Summary plots show data pooled from ≥2 independent experiments.

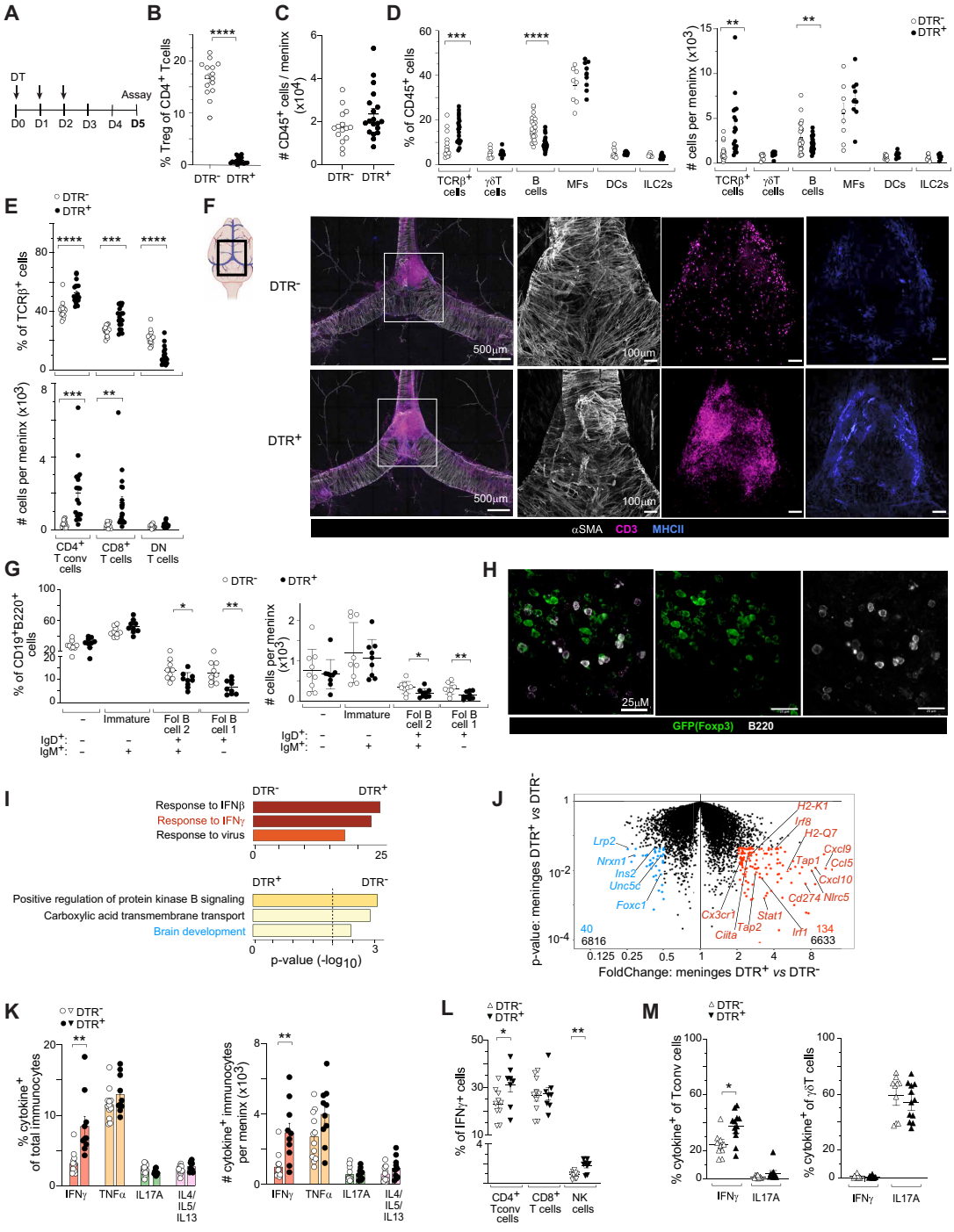

Fig. 3. Ablation of T_{regs} restrains the production of IFN-γ by meningeal lymphocytes. (**A**) T_{reg} depletion protocol. 6wk-old male DTR$^+$ and DTR$^-$ littermates were ip-injected with DT as indicated, and assays were performed on day 5 (D5) after the first injection. (**B**) Percentage of meningeal T_{regs}. n ≥ 15. (**C**) Total meningeal immunocyte counts. n 15. (**D**) Percentage (left) and numbers (right) of select immunocyte populations. n ≥ 8. (**E**) Percentage (upper) and numbers (bottom) of the major T cell subsets. n ≥ 15. (**F**) Imaging of meningeal sinuses from DT-treated DTR$^-$ and DTR$^+$ mice. Graphical representation showing the region of interest is shown to the left. Then a representative confocal image of the three indicated stains. Higher-power images of the white-squared region stained with, in order: αSMA for sinus structure, αCD3 for T cells and anti-MHCII for antigen presenting cells. (**G**) Percentage (left) and numbers (right) of meningeal B cell populations. n = 9. (**H**) Representative immunofluorescence image of T_{reg} and B cells in the meninges. (**I**) Pathway enrichment analysis via Metascape (*127*) of the genes differentially expressed in (J) [fold-change (FC) >1.5, p-value <0.05]. (J) Volcano plot of population-level RNA-seq comparing meninges in the presence and absence of T_{regs}. Annotated transcripts are those involved in the pathways highlighted in Fig. 3I (interferon signaling and brain development pathways). Triplicate samples. (**K**) Percentage (left) and numbers (center) of total cytokine-positive immunocytes from the dura mater. (**L**) Representation of the IFN-γ producers from (K). (**M**) Percentage of major cytokine-producing cells from the dura mater. DT, diphtheria toxin; DTR, DT receptor; MF, macrophages; NF, neutrophils; DCs, dendritic cells; ILC, innate lymphoid cells; Fol, follicular; other abbreviations as per Fig. 1. Mean ± SEM; p-values as per Fig. 1, by unpaired Student's *t* test [(B) to (E), (G), (K), (L), (M)]. Summary plots show data pooled from ≥2 independent experiments.

We examined the T_{reg}-depleted meningeal environment more comprehensively via whole-tissue RNA-seq of DTR^- and DTR^+ littermates. Meninges lacking T_{regs} were enriched in IFN-response signatures (both type I and II), while showing reduced expression of genes related to brain development (e.g. lower expression of *Lrp2, Nrxn1, Ins2, Unc5c, Foxc1*) (Fig. 3I, J). To confirm IFN induction and identify putative IFN-producing cells, we cytofluorometrically quantified meningeal cells expressing IFN-γ and other lineage-defining cytokines from DTR^- and DTR^+ mice (Fig. S5C). After T_{reg} depletion, immunocytes expressing IFN-γ, but not those making the other cytokines examined, were enriched in the meninges (Fig. 3K). $Foxp3^-$ $CD4^+$ conventional T (Tconv) cells and $CD8^+$ T cells were the major producers of IFN-γ in both the presence and absence of T_{regs}; loss of T_{regs} further increased IFN-γ production by $CD4^+$ Tconv and NK cells, although the contribution of NK cells remained low (Fig. 3L). Neither the fraction of T_H17 cells nor that of IL-17–producing γδT cells was increased in the meninges in the absence of T_{regs} (Fig. 3M).

To address whether meningeal T_{regs} drove these effects, we first injected an anti-CD25 monoclonal antibody (mAb) or an irrelevant anti-IgG control mAb into the cisterna magna and performed whole-tissue RNA-seq 72 hours later. Anti-CD25 injection is an alternative method to deplete T_{regs} (at least those that are $CD25^+$) [e.g. (*43–45*)]; intracisternal injection allows preferential delivery to the meninges while minimizing systemic spread (however, technical limitations permit only a single injection). CD25 was expressed on ~50-70% of all meningeal-T_{reg} subtypes (Fig. S5D) and none of the IFN-γ–producing cell types in the meninges expressed high levels of CD25 (Fig. S5E). In any case, ablation of such effector cells would have an opposite, anti-inflammatory, effect. As previously described, this protocol did not change total T_{reg} numbers but completely eliminated the $CD25^+$ T_{reg} component (determined using a different, non-competing anti-CD25 mAb) (Fig. S5F). Nonetheless, this method of T_{reg} ablation also elicited a clear response to IFN-γ in the meninges (Fig. S5G, H).

As a second approach, exploiting up-regulation of MHCI as a marker of IFN-γ sensing, we compared the time course of IFN-γ responsiveness in the meninges and spleen (Fig. S5I, J). In the meninges, up-regulation of MHCI expression was evident on both immunocytes and stromal cells by 24 hours after the first DT injection, while in the spleen, up-regulation was observed only at 72 hours [consistent with (*46*)] and only on stromal cells (Fig. S5K). Along with the short depletion protocol we employed, these two sets of findings argue that the punctual ablation of meningeal T_{regs} incited a local response, and the resulting immunological changes did not simply reflect systemic effects ensuing from loss of the circulating T_{reg} pool.

T_{regs} inhibit lymphocyte invasion of the brain parenchyma

Immunocytes within the dura mater, especially T cells, have a direct route of communication with the brain parenchyma (*2*). Moreover, the meninges are indispensable for proper brain function (*47*), with intrinsic roles in B cell differentiation (*48*, *49*), innervation (*50*), and defense against pathogens (*50*, *51*). Thus, we examined how the brain is affected by our previously employed punctual T_{reg} depletion protocol. More $CD45^+$ cells, particularly αβT and NK cells, were found in the brain parenchyma of perfused DTR^+ than DTR^- mice (Fig. 4A, B). There seemed to be no preference for $CD8^+$ vs $CD4^+$ T cells (Fig. S6A, B). Residual contamination by circulating cells (identified by intravascular labelling of blood cells with a fluorescent anti-CD45 mAb (*52*)) was limited to just 9.7% and 12.1% $CD45^+$ cells in the parenchyma and meninges, respectively (Fig. S6C).

To study the effects of T_{reg} depletion on brain T cells, we performed confocal microscopy on sections from four brain regions: the hippocampus, cingulate cortex, cortex region overlying the hippocampus, and thalamus (Fig. 4C). Ablation of T_{regs} resulted in more T cell accumulation in the hippocampus and, to a lesser extent, in the cingulate cortex but not in the other two brain regions examined (Fig. 4D). The T cells were scattered throughout the hippocampus (Fig. 4E). We also stained brain sections with a mAb recognizing cFos, an immediate-early marker of cell activation and thereby neuronal activity (*53*). $cFos^+$ cells were reduced in the hippocampus as a whole and in the cortex just above it but were specifically increased in the dentate gyrus (DG) of the hippocampus, a major site of adult neurogenesis (Fig. 4F; Fig. S6D).

For a comprehensive view of brain changes following T_{reg} depletion, we performed whole-tissue RNA-seq on four dissected brain regions: the cortex, hippocampus, thalamus plus hypothalamus (T&H), and cerebellum (Fig. 4G). Primarily in the hippocampus (Fig. 4H, I), but also to a lesser extent in the T&H and cortex regions (Fig. S6E, F), there was an increase in IFN-γ signaling pathways. In stark contrast, the cerebellum did not show an enrichment in these gene sets (Fig. S6E, F) even though transcripts encoding IFN receptors were amply expressed throughout the brain (Fig. S6G). Consistent with a localized induction of IFN-γ signaling pathways, the response of both total and IFN-γ–induced transcripts to punctual loss of T_{regs} in the meninges vs hippocampus revealed the former to temporally precede the latter (Fig. S6H). Hippocampi from DTR^+ mice also showed an enrichment for gene signatures indicative of reactive and disease-associated glia (*54–57*) coupled with a reduction in signatures associated with myelination, neuronal differentiation, and neurogenesis (*Gfap, Sox2, Ascl1, Hes1, Wnt2)* (Fig. 4J, Fig. S6I).

We employed several experimental approaches to examine the route by which T cells enter the brain upon T_{reg} depletion. First, the size of DT (~58 kD) should prevent it from penetrating the brain via the blood/brain barrier (BBB), arguing against a purely local effect due to a loss of the very few brain T_{regs}. In fact, brain T_{reg} numbers were not reduced with our T_{reg}-ablation protocol; rather they were increased, likely in response to the local inflammation (Fig. S7C). Second, we employed dyes of three different sizes – Evans blue (~960 D alone, ~67 kD when bound to albumin), FITC-Dextran (40 kD), and FITC-Dextran (70 kD) – to assess levels of BBB permeability. No BBB impairment was detected either in the whole brain parenchyma or the hippocampus (Fig. S7A, B). Third, we evaluated the contribution of T cells circulating through peripheral lymphoid organs by blocking their egress with FTY720, a functional antagonist of the S1P receptor. FTY720 prevented T cell accrual in the brains of DTR^+ and DTR^- mice to a similar degree (60-65%) (Fig. S7D, E), indicating that some brain T cells could infiltrate from the circulation, either directly or via the meninges, in response to T_{reg} ablation but that such recruitment was similar to that during homeostasis. Lastly, we examined the velum interpositum (VI), a double-layered invagination of the pia mater under the hippocampus known to be a site of immunocyte trafficking during inflammation (*58*). T cells were almost never found in the VI of DTR^- mice but were readily observed in parallel sections of their DTR^+ littermates (Fig. S7F).

The signals guiding T cell infiltration into the brain parenchyma remain unclear. Interestingly, we found that transcripts encoding CXCL14, a chemokine implicated in brain invasion by T cells during viral infections, stroke, and tumors (*59–61*), was upregulated in the hippocampus, primarily by astrocytes and RGL cells (Fig. S7G).

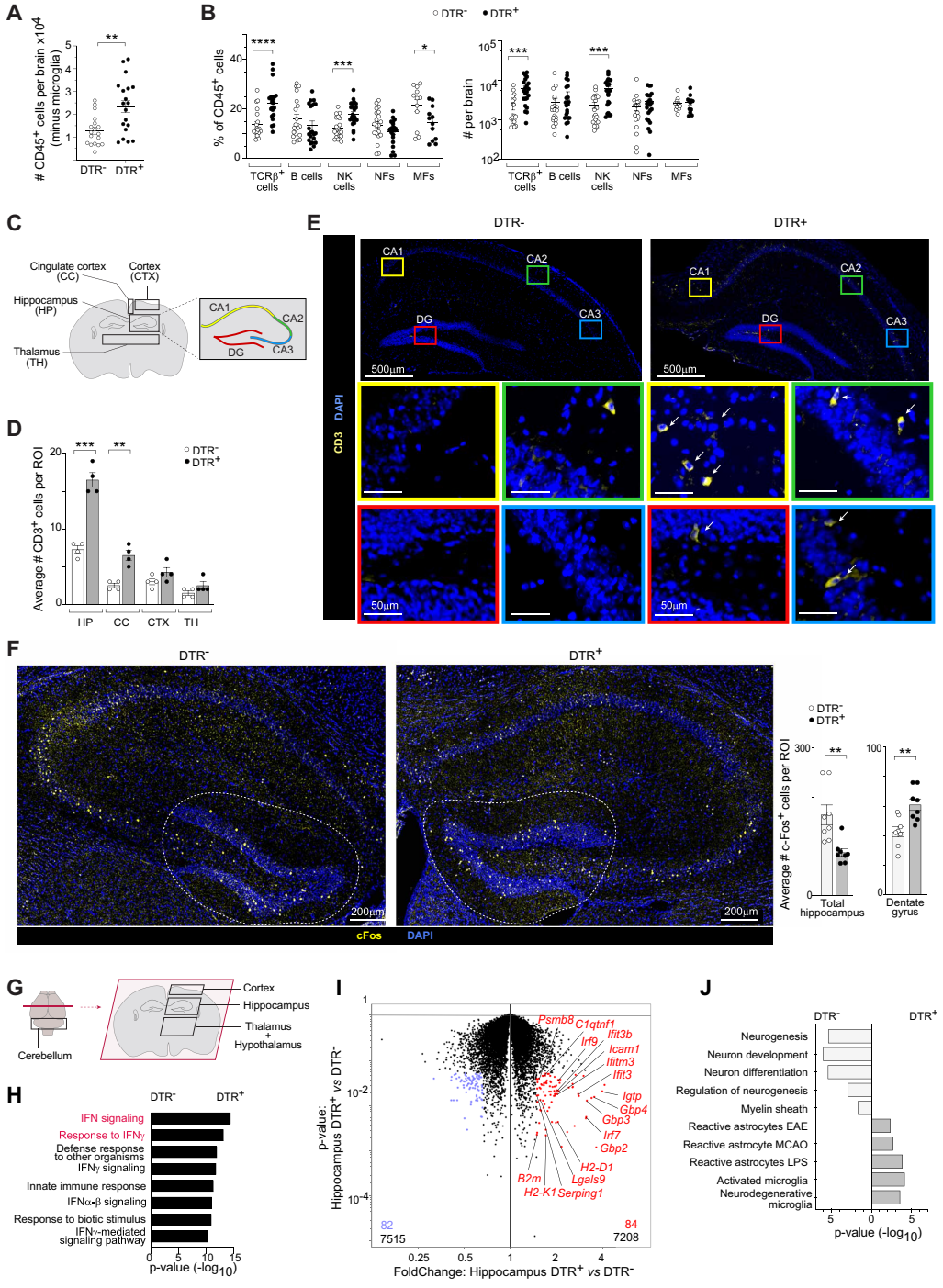

Fig. 4. T cells invade the brain parenchyma in the absence of T_{regs}. (**A-B**) Flow-cytometric analysis of the brain parenchyma of mice depleted of T_{regs} or not, as per Fig. 3A. Males mice aged 6 to 7 wks old. (A) Total immunocyte numbers. n ≥ 18. (B) Frequency (left) and numbers (right) of select immunocyte populations. n ≥ 11**.** **(C-E)** T cell invasion into the brain parenchyma after depletion of T_{regs} in DT-treated DTR^+ mice, as per Fig. 3A. (C) Diagrammatic representation of the brain with regions of interest delineated. Coronal section. (D) Quantification of the average $CD3^+$ T cells. n = 4**.** (E) Representative confocal images of coronal sections of the whole hippocampus. Top row: regions of interest. The quartet of higher power images below show anti-CD3 mAb (+DAPI) staining for T cells in each region of interest, framed in the colors corresponding to those of the top panel. Arrows point to T cells. (**F**) Left: representative confocal images of the hippocampus' cFos staining pattern in the presence (left) or absence (right) of T_{regs}. The dotted line delimits the DG. Right: quantification of $cFos^+$ cells in the hippocampus and DG. n ≥ 8. (**G-J**) Whole-tissue RNA-seq analysis of brain regions from mice depleted of T_{regs} or not, as per Fig. 3A. (G) Diagram showing regions of interest. (H) Pathway-enrichment analysis via Metascape (*127*) of the differentially expressed transcripts from (I) [FC>1.5; p-value<0.05]. (I) Volcano comparing DTR^+ and DTR^- hippocampus. Annotated genes are those involved in pathways highlighted in (H) (interferon signaling and response to IFN-γ). Triplicate samples. (J) Specific analysis via Gene Ontology (GO) and GSEA (MsigDB) database of pathways related to glial activation and hippocampal functions. DG, dentate gyrus; CA, Cornu Ammonis; other abbreviations as per Fig. 3. Mean ± SEM; p-values as per Fig. 3. Mean ± SEM; p-values as per Fig. 1, by unpaired Student's *t* test [(A), (B), (D), (F)] or chi-square test [(H), (J)]. Summary plots show data pooled from ≥2 independent experiments.

Thus, meningeal T_{regs} serve as gatekeepers to the brain parenchyma. In their absence, lymphocyte invasion of the brain occurs, likely by multiple routes.

T_{regs} restrain glial cells in the hippocampus

Hippocampal glial cells, both microglia and astrocytes, are vital for brain development and function (*62*), including removal of newborn neurons undergoing apoptosis, regulation of the survival and proliferation of new neurons, regulation of neuronal stem-cell proliferation and differentiation (*63*) and control of memory formation (*64*–*66*). To explore the state of glia after punctual T_{reg} depletion (as per Fig. 3A), we performed confocal microscopy on dentate gyrus sections. $Iba1^+$ microglia acquired the morphology of activated cells, with reduced arborization, including fewer branches and processes per cell, fewer branches per process, and shorter processes (Fig. 5A). The high abundance and low heterogeneity of adult hippocampal microglia (*67*) permitted us to sort them from DTR^- and DTR^+ littermates and perform population-level RNA-seq. We observed over-representation of both disease-associated (*56*) and damage-associated (*57*) microglia signatures in microglia from DTR^+ mice (Fig. 5B). In addition, pathway analysis showed an enrichment for terms related to anti-viral responses, cytokine secretion, and responses to IFN-γ (Fig. S8A). $GFAP^+$ astrocytes in the hippocampus exhibited a parallel reduction in arborization in T_{reg}-deficient mice (Fig. 5C), suggesting widespread glial activation in the hippocampus.

We also performed scRNA-seq analysis of the hippocampus from DTR^- and DTR^+ mice (in duplicate), excluding mature neurons ($Thy1^+$) and microglia ($CD45^+$) so as not to obscure differences in rarer cell types. After quality control, we retained a total of 10,234 cells with an average of 2,182 unique transcripts per cell. Dimensionality reduction, unsupervised clustering, and signature analysis revealed all of the major cell types known to participate in the neuronal stem-cell niche (*68*) (Fig. 5D) in both conditions (Fig. 5E). Although the same cell types were present in hippocampi from DTR^- and DTR^+ mice, their distribution differed in the absence of T_{regs}, the hippocampus showing an increase in astrocytes and oligodendrocyte precursor cells (OPCs), the latter in association with a reduction in oligodendrocytes (Fig. 5E).

Re-clustering of the astrocytes revealed four subtypes (Fig. 5F), the validity of which was confirmed by a heatmap of the twenty genes most differentially expressed by each subcluster (Fig. S8B). Given the identity of differentially expressed genes among subclusters, we termed the four subtypes: immature, pro-neurogenic, reactive, and active, as per (*69*, *70*). Upon punctual T_{reg} ablation, the hippocampal astrocyte landscape evolved from primarily immature and pro-neurogenic to reactive (Fig. 5G). An analogous procedure was applied to the OPC cluster, yielding two previously characterized subtypes: pro-myelinating (OPC2s) and pro-inflammatory (OPC1s) (*71*) (Fig. 5H, Fig. S8C, D). Loss of T_{regs} provoked a switch to the pro-inflammatory phenotype (Fig. 5I). Thus, T_{regs} promote an unreactive glial landscape in the hippocampus at homeostasis.

T_{regs} regulate hippocampal neurogenesis

The hippocampus is one of the few brain regions where new neurons are generated in adult mice and humans (*72*, *73*). Hippocampal neurogenesis is required for effective learning and memory formation throughout adulthood (*74*, *75*). Hippocampal pluripotent progenitors, i.e. radial-glia-like (RGL) cells, reside in the subgranular zone (SGZ) of the DG (Fig. S9A). As they differentiate into neurons, RGL cells proliferate and migrate axially, becoming intermediate progenitor cells for neurons (nIPC). nIPCs migrate vertically into the granular cell layer (GCL), where they are known as neuroblasts. Neuroblasts undergo a complex series of changes that resolves in either cell death or integration into the neuronal circuitry (*72*, *76*).

Re-clustering neuronal cells from the scRNA-seq data of Fig. 5D revealed 5 subtypes: early progenitors, proliferating IPCs, nIPCs, neuroblasts, and a few contaminating OPCs (Fig. S9B). Loss of T_{regs} (in DTR^+ mice) resulted in a very slight decrease in early progenitor cells and a small increase in nIPCs (Fig. S9B). The transcriptomes of the various subtypes were very similar in the presence and absence of T_{regs} (Fig. S9C); although, suggestively, cells from the early-progenitor or nIPC clusters of DTR^+ mice showed small reductions in several transcripts encoding proteins crucial for stem-cell identity (e.g. *Sox9, Hes1, Fezf2, Neurod1, Hmgn2*) (*74*, *77*–*81*), differences that were no longer evident at the neuroblast stage.

To more precisely examine potential changes undergone by early neural progenitors in the absence of T_{regs}, we re-clustered them in isolation, yielding three discernable and replicable subtypes (Fig. S9D, E). A heatmap of the most differentially expressed genes confirmed the clustering (Fig. S9F), and the gene identities prompted us to designate the subtypes "RGL cells," "activated neural stem cells" (aNSCs), and "quiescent neural stem cells" (qNSCs). These designations were supported by heatmaps of transcripts encoding the key RGL cell identifiers, *Gfap* and *Sox2* (Fig. S9G), and by overlaying published signatures of qNSCs and aNSCs (*82*) on the UMAP (Fig. S9H). RNA-velocity analysis suggested with high confidence that RGL cells could differentiate into either qNSCs or aNSCs in the presence of T_{regs} (Fig. S9I, left), as has been reported (*82*), which was further supported by Partition-based Graph Abstraction (PAGA) (Fig. S9I, left). Punctual ablation of T_{regs}, resulted in loss of most of the velocity vectors (and, consequently, loss of directional confidence), suggesting a block of both of these differentiation routes (Fig. S9I, right), Consistent with this finding, the biggest change in the RGL-cell compartment subsequent to T_{reg} ablation was an increase in the fraction of $Gfap^+Sox2^+$ progenitor cells (Fig. S9J). In addition, the transcriptomes of hippocampal RGL cells from T_{reg}-depleted mice were relatively enriched in transcripts associated with aerobic respiration [a feature of NSC activation (*72*, *83*–*85*)], stress, and apoptosis. They also expressed low levels of transcripts associated with evolving RGL cells, such as radial-glia-like cell differentiation and gliogenesis (*86*, *87*) (Fig S9K). Gene-Set-Enrichment analysis (GSEA) confirmed this reduction in pathways associated with neurogenesis and gliogenesis in RGL cells from mice lacking T_{regs} (Fig. S9L). Notably, these pathways did not come up when comparing 10 randomly re-shuffled datasets.

T_{regs} protect RGL cells from IFN-γ–induced death and promote short-term memory

As an orthogonal approach to validate the observed changes in neurogenesis after T_{reg} depletion, we performed quantitative stereological imaging of the DG, examining both the SGZ, which encompasses RGL cells, and the GCL, which hosts immature and mature neurons (Fig. 6A). There was no evidence of macro-morphological abnormality in the absence of T_{regs} as we did not observe any differences in either GCL volume (Fig. 6B) or SGZ area (Fig. 6C). There were also no significant differences in the number of immature (DCX+) neurons (Fig. 6D, Fig. S10A), and only a small increase in cellularity of the GCL zone (mostly mature neurons) (Fig. 6E). Focusing on the

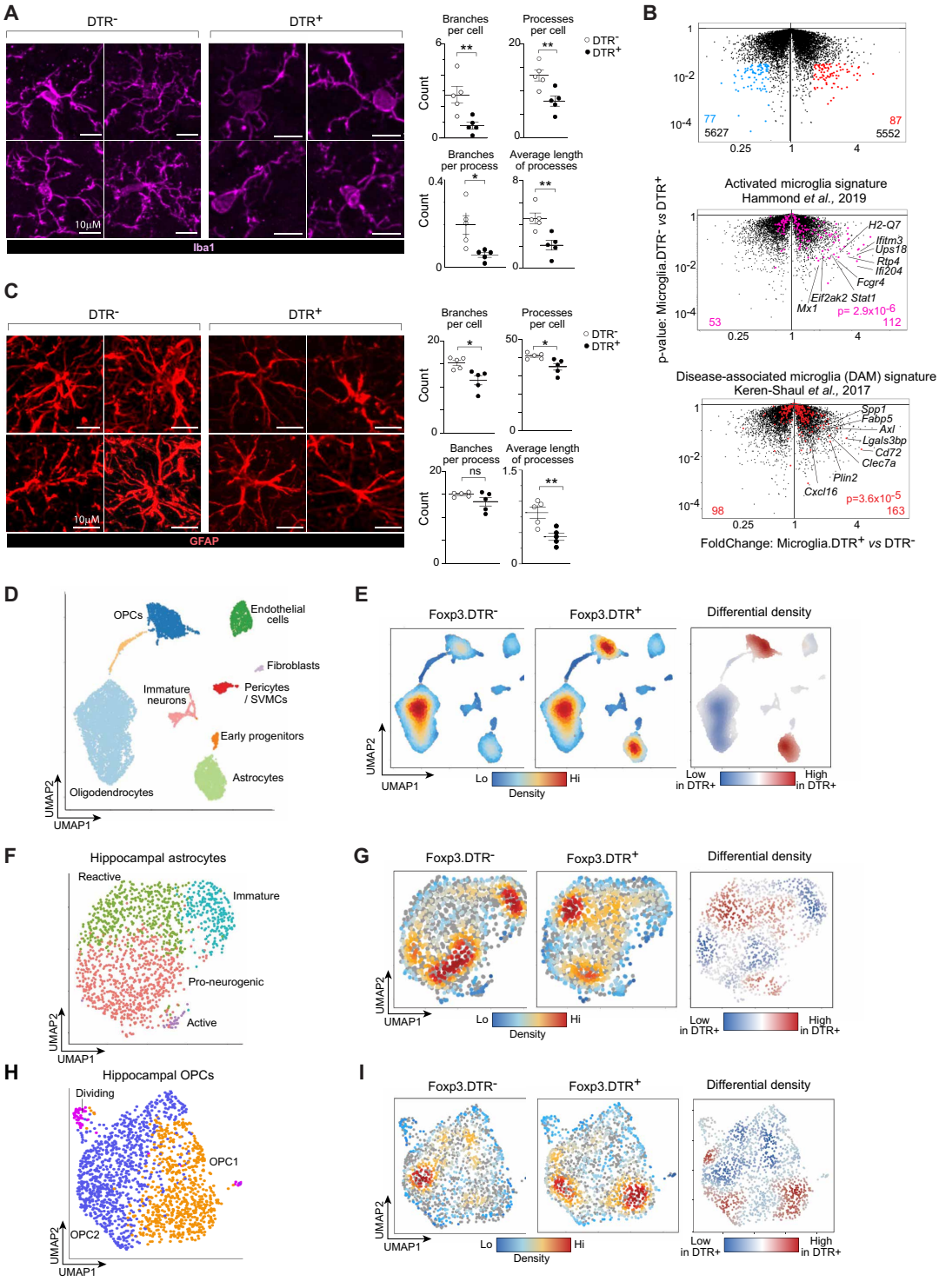

Fig. 5. T_{regs} control hippocampal glial cells. (**A**) Left: representative confocal images of DG microglia (Iba1+); right: summary quantification of classical morphological changes in activation. n = 5. (**B**) "Activation upon demyelination" (*56*) (top) and "Disease-associated" (*55*) (bottom) microglia signatures are red-highlighted on a volcano plot comparing transcripts expressed in sorted hippocampal microglia from DT-treated DTR- versus DTR+ mice. Duplicate samples. (**C**) Same as (A), but with images of astrocytes (GFAP+). (**D-I**) scRNA-seq analyses of dissected hippocampal cells depleted of mature neurons (Thy1+) and microglia (CD45+). Duplicate samples. (D) UMAP representation. (E) Normalized local cell densities on the UMAP space from DTR- (left) or DTR+ (center) mice. Density differential map between the two genotypes (right). (F) UMAP representation of re-clustered astrocytes (light green) from (D). (G) Same as (E) except specifically for the astrocyte cluster (light green) in (D). (H-I) Same as (F) and (G) except the OPCs (blue) from (D) were re-clustered. OPCs, oligodendrocyte precursor cells; SVMCs, smooth vascular muscle cells; other abbreviations as per Fig. 3. Mean ± SEM; p-values as per Fig. 1, by unpaired Student's t test [(A), (C)] or chi-square test [(B)]. Summary plots show data pooled from ≥2 independent experiments.

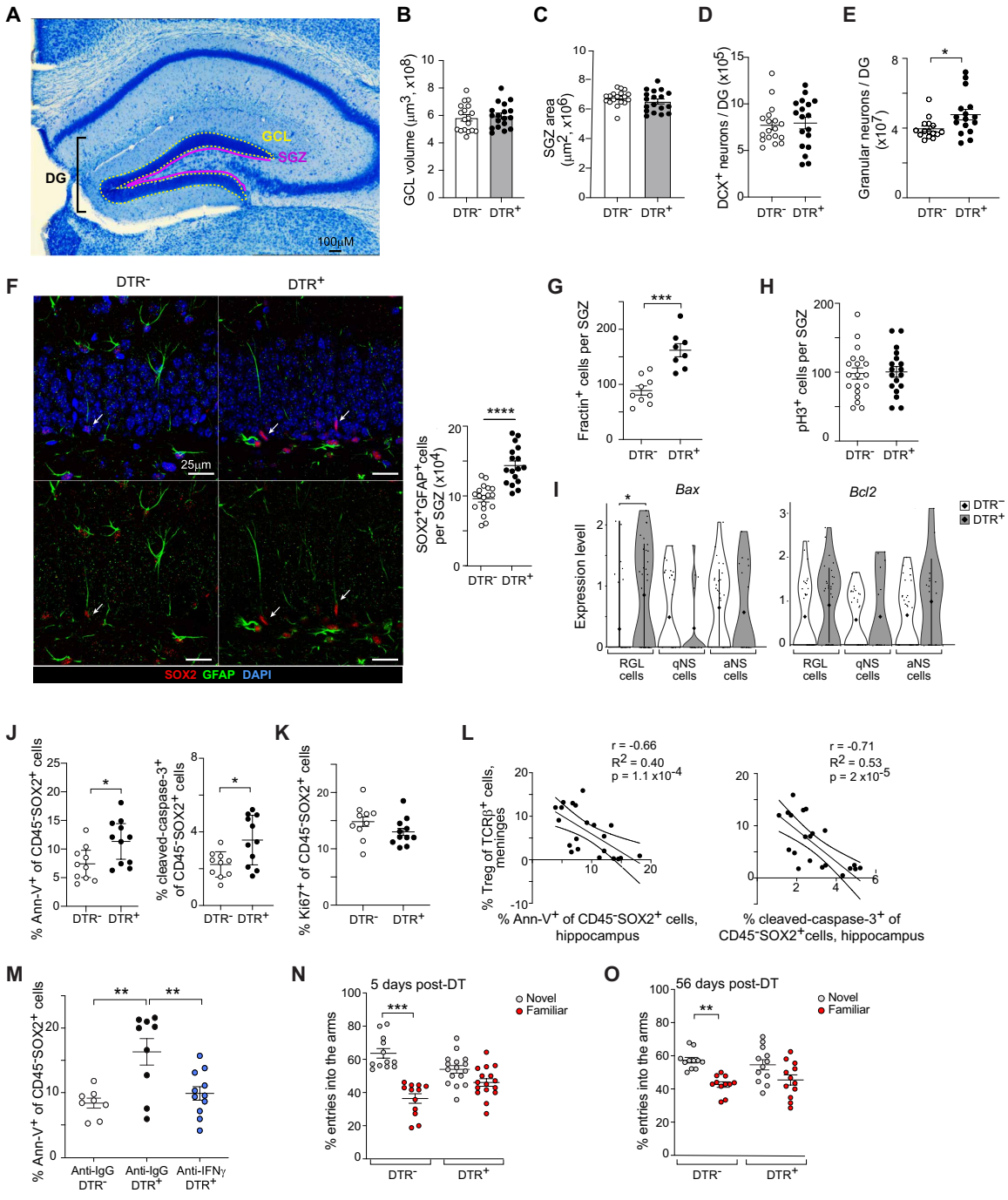

Fig. 6. T_{reg}-mediated protection of RGL cells from IFN-γ–induced death and against impairments to short-term memory. (**A-O**) DTR$^+$ and DTR$^-$ littermates (6 – 7wks old) were injected with DT as per Fig. 3A and analyzed on day 5 after the first injection. n = 18 for (B)-(F). (A) Representative image of Nissl staining of the hippocampus. Relevant DG anatomical structures: SGZ (solid magenta line) and GCL (dotted yellow line). (B) GCL volume. (C) SGZ area. (D) Histological quantification of immature (DCX$^+$) neurons. (E) Histological quantification of granular neurons. (F) Left and center: representative confocal images of RGL cells (arrows) from DTR$^-$ and DTR$^+$ littermates. All markers are shown in the upper panels, while DAPI staining has been removed in the lower panels. Right: summary quantification of RGL cells per SGZ. (G) Histological quantification of Fractin+ cells per SGZ. n ≥ 8. (H) Histological quantification of pH3+ cells per SGZ. n ≥ 18. (I) Violin plot of *Bax* and *Bcl2* transcription expression from the clusters delimited in Fig S8D. (J) Flow-cytometric quantification of the frequency of RGL cells (CD45$^-$SOX2$^+$) expressing death markers: Annexin-V$^+$ (left) and cleaved-caspase-3$^+$ (right). n ≥ 10. (K) Percentage of Ki-67$^+$CD45$^-$SOX2$^+$ cells. n = 11. (L) Correlation between the meningeal T_{reg} frequency and the frequency of death markers on the RGL cells (CD45$^-$SOX2$^+$): Annexin-V$^+$ (left) and cleaved-caspase-3$^+$ (right). n = 21. (M) Flow-cytometric analysis of Annexin-V$^+$ RGL (CD45$^-$SOX2$^+$) cells from DT-treated DTR$^+$ and DTR$^-$ mice treated with an anti-IFN-γ or isotype-control mAb. n ≥ 8. (N) Frequency of entries by individual mice into the familiar (red dots) versus novel (grey dots) arms of the Y-maze 5 days after the initial DT injection. n ≥ 12. (O) Same as (M), except the readout was 56 days after the initial DT injection. n ≥ 11. DG, dentate gyrus; GCL, granular cell layer; SGZ, subgranular zone; IFN, interferon; other abbreviations as per Fig. 6. Mean ± SEM; p-values as per Fig. 1, by unpaired Student's *t* test [(B) to (H), (J), (K), (N), (O)], one-way ANOVA [(M)], simple linear regression [(L)], or Wilcoxon test [(I)]. Summary plots show data pooled from ≥2 independent experiments.

SGZ, we found more RGL cells ($SOX2^+GFAP^+$) in DTR^+ mice (Fig. 6F), consistent with our scRNA-seq data (Fig. S9J). Such an increase in RGL cells without changes in immature neurons prompted us to assess their state. There were more dead cells ($Fractin^+$) in the SGZ of DTR^+ mice (Fig. 6G), but no increase in proliferation [phosphorylated histone $(pH)3^+$] (Fig. 6H). This observation was substantiated by scRNA-seq data demonstrating an increase in transcripts encoding pro-apoptotic BAX in the absence of T_{reg}, with no change in transcripts specifying anti-apoptotic BCL2 (Fig. 6I) nor enrichment of proliferation signatures (Fig. S9K). Flow-cytometric analysis (Fig. S10B) also confirmed that RGL cells ($CD45^-SOX2^+$) from DTR^+ mice were more frequently undergoing apoptosis (Annexin-V^+ and cleaved-caspase-3^+) in the absence of T_{regs} (Fig. 6J), a change not compensated for by increased proliferation (Fig. 6K). More mature neurons showed the opposite dynamics ($CD45^-SOX2^-$) (Fig. 6E, Fig. S10C, D). Importantly, there was a significant negative correlation between the fraction of T_{regs} in the meninges and the fraction of dead RGL cells in the hippocampus (Fig. 6L).

The other major adult neurogenic niche is located in the ventricular-subventricular zone (V-SVZ), which plays a crucial role in generating new olfactory neurons (*88*). Following T_{reg} ablation, there were no significant changes in the frequency or cell death of NSC or neural progenitor populations (B1 or B2 cells), nor of mature neurons and their niche (C or ependymal cells) in the V-SVZ (Fig. S10E, F). Additionally, there was no evidence of T cell infiltration within the V-SVZ (Fig. S10G), emphasizing once again the localized nature of the changes following punctual loss of T_{regs}.

Because loss of T_{regs} resulted in a strong enrichment of IFN-γ signaling pathways in the hippocampus, we questioned whether IFN-γ was involved in neuronal cell death. IFN-γ has been reported to have a concentration-dependent effect on RGL cells, mostly in *in vitro* settings (*13*, *29*, *85*, *89*–*94*). Hippocampal RGL cells expressed both subunits of the IFN-γ receptor (Fig. S10H). Furthermore, IFN-γ response genes were specifically enriched in the RGL-cell cluster of Fig. S9D (Fig. S10I). We co-administered an anti-IFN-γ mAb or an irrelevant anti-IgG control mAb 8 hours before the first DT injection of the T_{reg} ablation protocol and then every other day until day 5. Neutralization of IFN-γ was indeed able to reduce the fraction of dead RGL cells in the hippocampus to the levels of T_{reg}-replete mice (Fig. 6M), without affecting death of non-RGL cells (Fig. S10J). Despite the ability of anti-IFN-γ to curb death, the $CD4^+$ and $CD8^+$ effector T cell populations still expanded in the meninges (Fig. S10K-L) and in the hippocampus (Fig. S10M), indicating that expansion of T effector cell populations was IFN-γ–independent. To determine whether IFN-γ had a direct impact on RGL-cell survival, we generated neurospheres from the hippocampus of 3 to 10-day-old mice (*95*, *96*). When rIFN-γ was added at the initiation of neurosphere formation, there was a dose-dependent reduction in live RGL cells (Fig. S10N, O) as well as the appearance of dead-cell blebs a week later (Fig. S10Q), likely signaling a reduction in the initial pool of hippocampal RGL cells. Parallel results were obtained when preformed neurospheres were treated with rIFN-γ (Fig. S10P).

Lastly, we examined whether the inhibition of RGL-cell differentiation provoked by loss of T_{regs} had a functional impact on the hippocampus. Short-term spatial-reference memory, which is dependent on the hippocampus (*74*), was tested by placing a mouse in a Y-maze with one arm closed off during a training period. After a resting period, the mouse should remember which arm it already explored and visit it less frequently than the unexplored arm. Whereas DTR^- mice did enter the novel arm more often, DTR^+ mice did not show a significant preference, indicating an inability to remember what they had previously explored (Fig. 6N). Surprisingly, this defect was maintained for at least 8wks after T_{reg} depletion, demonstrating that the functional damage to the hippocampus endures over time (Fig. 6O). At neither timepoint was there a change in locomotion in the absence of T_{regs} (Fig. S10R).

T_{regs} control IFN-γ levels by depriving T and NK effector cells of IL-2

We next addressed the mechanism(s) underlying T_{reg} control of T- and NK-cell activities in the meninges and brain parenchyma, in particular their production of IFN-γ. We previously reported that punctual depletion of local T_{regs} unleashes proliferation of, and IFN-γ production by, NK and T cells in the pancreatic islets by depriving effector cells of IL-2 via CD25-dependent competition (*97*). We hypothesized that a similar process could occur in the meninges upon T_{reg} depletion. In support of this notion, near-total ablation of $CD25^+$ T_{regs} using an anti-CD25 mAb (with a much milder effect on total T_{reg} numbers) induced a meningeal IFN-γ response that closely mimicked that achieved by punctual depletion of the entire T_{reg} compartment (Fig. S5D-F).

IL-2 binding activates a STAT5-directed transcriptional program (*98*). Staining meningeal immunocytes from wild-type mice revealed frequent expression of phosphorylated STAT5 (pSTAT5) by $CD4^+$ Tconv, $CD8^+$ T, NK and B cells, suggestive of IL-2 sensing, but not by γδT cells or MFs. Littermates punctually depleted of T_{regs} showed increased pSTAT5-positivity for only $CD4^+$ Tconv, $CD8^+$ T, and NK cells, pointing to an IL-2 boost (Fig. 7A). This interpretation was supported by the induction of a previously published IL-2-response signature in NK cells and $CD4^+$ Tconv cells 24 hours after a single injection of DT into *Foxp3.Dtr*$^+$.*Gfp*$^+$ mice (Fig. S11A), less strongly for the T cells likely due to their slower activation kinetics (*99*, *100*).

If T_{reg} control of IL-2 availability is indeed important for guarding homeostasis of the meningeal immune system, co-incidental T_{reg} depletion and neutralization of IL-2 should prevent the usual expansion of and IFN-γ production by meningeal T and NK cell populations. Neutralization of IL-2 in the presence of T_{regs} (as per the protocol depicted in Fig. 7B) did not significantly change the numbers of total meningeal T_{regs} (Fig. S11B), total immunocytes (Fig. S11C), or any lymphocyte subset examined (Fig. 7C). In contrast, neutralizing this cytokine in littermates concomitantly depleted of T_{regs} strongly reduced expansion of the total, $CD4^+$ Tconv and $CD8^+$ T cell populations (Fig. 7C). Similarly, neutralization of IL-2 in mice hosting T_{regs} had little effect on immunocyte accumulation within the brain parenchyma, while it inhibited the typical expansion of brain $CD8^+$ T and NK populations in T_{reg}-deficient littermates (Fig. 7D and Fig. S11D, E). IL-2 neutralization also reduced the death of hippocampal RGL cells following T_{reg} depletion (Fig. 7E) without impacting their cell-cycle entry (Fig. 7F). In addition to the lack of an anti-IL-2 effect in T_{reg}-replete mice, the specificity of these observations is supported by the absence of splenic T and NK population expansion in anti-IL-2-treated T_{reg}-deficient mice (Fig. S11F-H).

Injection of IL-2/anti-IL-2 complexes containing the antibody clone S4B6 has been shown in several systems to highly preferentially agonize the low-affinity IL-2R dimer expressed by $CD4^+$ Tconv, $CD8^+$ T and NK cells but not the high-affinity IL-2R trimer expressed primarily by T_{regs} (*97*, *98*, *101*); in contrast, injection of IL-2/anti-IL-2 complexes containing the antibody clone JES6 better agonizes CD25-containing IL-2R, thereby preferentially expanding T_{reg} populations

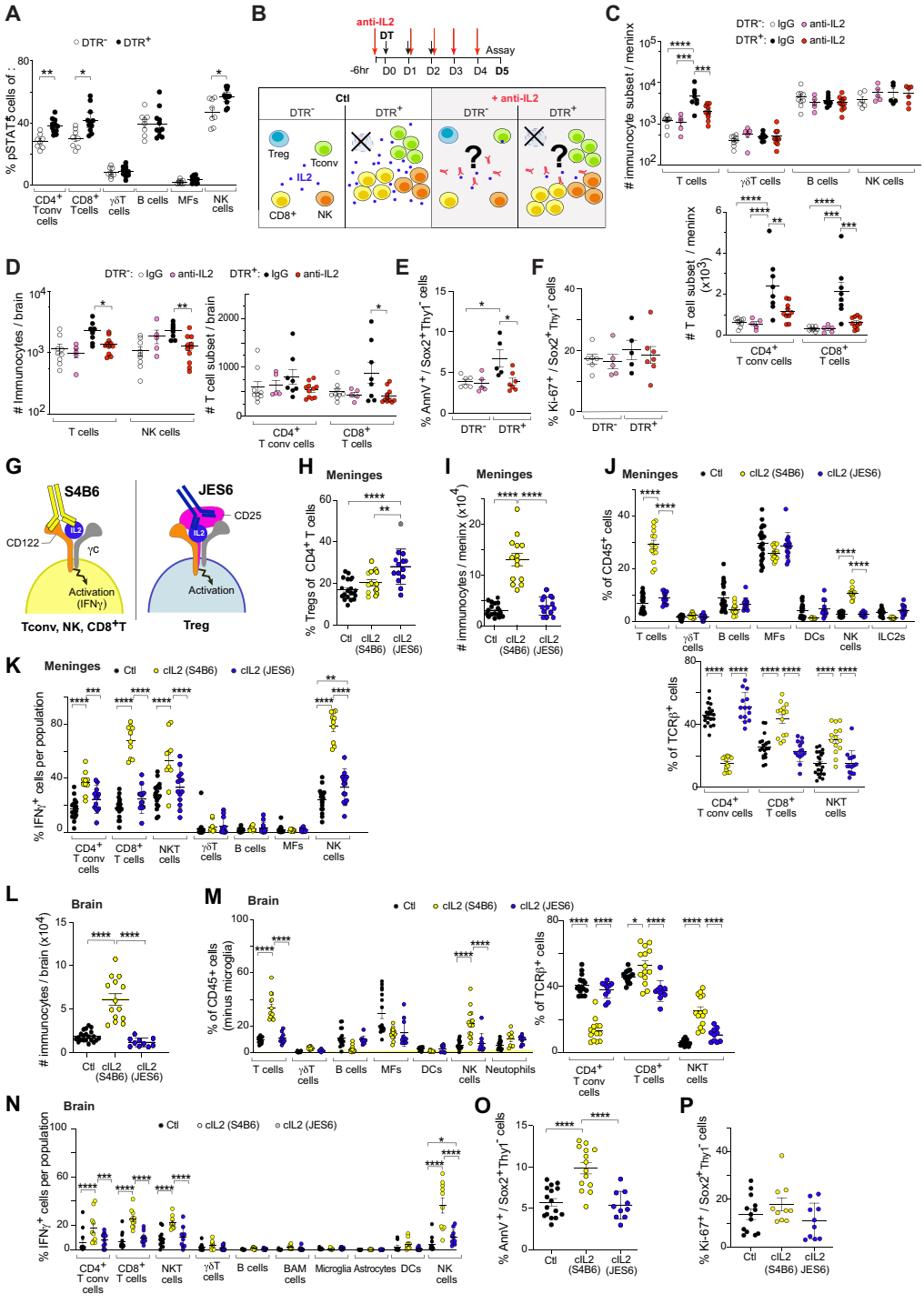

Fig. 7. Dura mater IL-2 availability is fine-tuned by T_{regs}. (**A**) Frequency of pSTAT5+ select immunocyte populations in mice with or without T_{reg} depletion. n ≥ 8 (**B-F**) Flow-cytometric quantification of DTR^+ and DTR^- male littermates (6-7wks old) ip-injected with DT and anti-IL2 or isotype control mAb. n ≥ 5. (B) Anti-IL2 blocking protocol and schematic of the different conditions. (C) Numbers of select meningeal immunocyte populations (top) and T cell subsets (bottom). (D) Same as (C) except for the brain parenchyma. (E) Frequency of Annexin-V^+ hippocampal RGL cells. (F) Frequency of Ki-67^+ hippocampal RGL cells. (**G-P**) Flow-cytometric analysis of the duramater and brain parenchyma of B6 WT littermate males (6 – 7wks old) after ip-injection of PBS (black), JES6-containing complex IL2 (cIL2) (gray) or S4B6-containing cIL2 (white). n ≥ 14. (G) Schematic representation of the both cIL2 and their target cells (H) Percentage of meningeal T_{regs}. (I) Total meningeal immunocyte counts. (J) Percentage of meningeal select immunocyte populations (left) and T cell subsets (right). (K) Percentage of IFN-γ^+ immunocyte populations. n ≥ 10. (L) Total brain immunocyte counts. n ≥ 10. (M) Same as in (I) except for the brain. n ≥ 10. (N) Same as in (J) except for the brain. n ≥ 10. (O) Frequency of Annexin-V^+ hippocampal RGL cells. n ≥ 10. (P) Frequency of Ki-67^+ RGL cells. n≥10. Mean ± SEM, p-values as per Fig. 1, by unpaired Student's *t* test [(A)], one-way ANOVA [(E), (F), (H), (I), (L), (O), (P)], two-way ANOVA [(C), (D), (J), (K), (M), (N)]. For simplicity, only relevant statistical differences are shown. Summary plots show data pooled from ≥2 independent experiments.

(Fig. 7G). Indeed, the meningeal T_{reg} pool was not expanded 3 days after injection of IL-2/S4B6 complexes but was increased by parallel injection of IL-2/JES6 complexes (Fig. 7H). In contrast, there was a large increase in total meningeal immunocytes after injection of S4B6-containing, but not JES6-containing, complexes (Fig 7I), the largest changes being among T and NK cells (Fig. 7J). There was also a striking increase in the fractions of T and NK cells expressing IFN-γ (Fig 7K). The brain parenchyma showed parallel changes with IL-2/S4B6 vs IL-2/JES6 complex injection: more total immunocytes (Fig. 7L), particularly T and NK cells (Fig. 7M) and an expansion of the IFN-γ^+ T and NK populations with S4B6-containing complexes (Fig. 7N). Moreover, there was more hippocampal RGL-cell death after injection of S4B6-containing complexes, with no changes in the fraction of dividing cells (Fig 7O, P).

On the basis of these experiments, we propose the following scenario (Fig. S12): In unperturbed wild-type mice, meningeal T_{regs} keep the activation, proliferation, IFN-γ production and parenchymal infiltration of T and NK cell effectors in check by out-competing them for limiting amounts of the growth and survival factor, IL-2. Upon punctual loss of T_{regs}, T and NK populations become activated, rapidly expand, and potently produce IFN-γ. They also develop the capacity to invade the brain parenchyma, where they activate glial cells, especially in the hippocampus, and promote death of hippocampal RGL cells, likely both directly and indirectly, thereby compromising their differentiation and short-term spatial-reference memory.

DISCUSSION

Several studies over the past several years have revealed the richness of the meningeal immune system in mice and have uncovered the important roles they can play in brain responses to aging, injury, or infection (*34*, *102*). Most of these explorations concentrated on the cellular and molecular impacts of various myeloid (MF) or lymphoid (T or B cell) effector populations. Our study, in contrast, focused on an essentially uncharacterized population of meningeal T_{regs} and the regulatory mechanisms they mobilize to safeguard brain homeostasis at steady state.

Besides controlling meningeal immunocyte responses, including impeding their access to the brain parenchyma, T_{regs} exerted widespread influences on the hippocampus. Upon acute loss of T_{regs}, the entire hippocampal region switched to a reactive, pro-inflammatory state, without evidence of the compensatory dampening mechanisms reported to arise in more progressive brain insults (*57*, *103–105*). RGL cells underwent the most dramatic changes, including differentiation blockade and death induction. To some extent, these effects may have resulted from the profound changes in glial cells known to promote neurogenesis (*68*, *106–108*). As discussed below, the RGL-cell changes almost certainly also reflected direct influences of IFN-γ. Regardless, T_{reg} depletion appeared to leave a "scar" in the hippocampus, leading to a persistent functional defect in short-term memory formation. Notably, a pattern of hippocampal changes very similar to that induced by punctual ablation of T_{regs} was recently observed in several human neurodegenerative diseases (*73*).

How do meningeal T_{regs} supervise the RGL cell niche? Compared with their lymphoid-organ counterparts, meningeal T_{regs} preferentially express a number of transcripts encoding proteins capable of influencing neurogenesis and brain function: *Il10*, *Wnt3*, *Hpgds, Psap* or *Ptgs1,* amongst others (*24–27*, *109*). And, there is precedent for meningeal cytokines diffusing into the brain and having profound impacts on cognitive behavior (*8–11*, *16*, *17*). However, our data highlight a different scenario: meningeal T_{regs} kept local IFN-γ–producing T and NK cells in check. Punctual ablation of T_{regs} led to rapid production of IFN-γ in the meninges, which ultimately resulted in RGL-cell death and sustained defects in neurogenesis within the DG.

The mechanisms(s) by which effector lymphocytes accumulate in the brain parenchyma upon T_{reg} depletion seem complex and their definitive elucidation will almost certainly require sophisticated experimentation. Here, we established that the proliferation of brain effector lymphocytes in response to depletion of T_{regs} in their vicinity or the loss of BBB integrity were probably not major elements. Instead, recruitment of circulating cells, either directly or by way of the meninges, and migration from the meninges to the hippocampus through the VI were likely to be involved.

We were struck by the similar profile of immunocytes that infiltrated the hippocampus (or the brain more generally) in the T_{reg}-depletion model and that reported to occur with aging or neurodegeneration in mice and humans. Like the loss of T_{regs}, aging is associated with increased levels of IFN-γ (*110*), coupled with T and NK cell invasion of the brain parenchyma (*111–113*). Relatedly, T cells have been increasingly implicated as key pathogenic agents in human and mouse neurodegenerative diseases such as Parkinson's disease, Lewis body dementia, and AD (*114–118*). For example, in a mouse model of AD, T cells, especially $CD8^+$ T cells, producing IFN-γ infiltrated the brain parenchyma, in particular the hippocampus, and were a major driver of disease progression (*116*). Intriguingly, in AD patients, T_{regs} were one of the immunocyte subsets collected from the cerebrospinal fluid that was most changed in comparison with those from healthy controls (*119*). But how and why these pathogenic, clonally expanded T cells access the brain parenchyma has remained unclear.

The fact that many of our experiments entailed organismal depletion of $Foxp3^+$ cells raises the question of whether the effects we observed primarily reflect a local or systemic loss of T_{regs}. Several observations argue that depletion of T_{regs} in the meninges was responsible for the defects manifest in mice rendered T_{reg}-deficient via our standard protocol. First, we performed assays quite a short time after the depletion protocol in order to mitigate systemic effects. Second, injection of an anti-CD25 mAb into the cisterna magna, a means to remove T_{regs} that is less inflammatory (*44*) and is meninges-preferential (*33*), provoked meningeal changes very similar to those observed upon DT-mediated T_{reg} depletion. Third, a very early time course analysis revealed a meningeal response to IFN-γ that was earlier and encompassed more cell types than did the splenic response (as a systemic-response indicator). And, lastly, perturbations of the brain parenchyma were localized to specific functional regions, notably the hippocampus, and were absent from others, e.g. the cerebellum. A striking illustration of this point were the effects on adult neural stem/progenitor cells in the hippocampal but not V-SVZ niche. Nonetheless, we cannot completely rule out any systemic effects from the T_{reg}-depletion protocol, via circulation of either cells or mediators. Nor can we completely rule out an input from the leptomeninges or choroid plexus, although this seems unlikely given that they host much fewer (15-fold and 29-fold less, respectively) T_{regs} than the dura does. Regardless, the salient finding of our study is that T_{regs} safeguard brain homeostasis in healthy mice.

MATERIALS AND METHODS

Study design

This study aimed to assess the role of regulatory T cells (T_{regs}) in the dura mater of the mouse meninges in maintaining brain homeostasis. We employed confocal imaging, flow cytometry, population-level RNA-seq and single-cell RNA/*Tra/b-seq* of meningeal T_{regs} to explore their representation, phenotype, putative functions and heterogeneity. Then we used an acute depletion system to remove T_{regs} and examine the effects in the meninges and brain parenchyma. Finally, we performed loss-of-function experiments, using blocking antibodies (anti-IFN-γ and anti-IL-2), and gain-of-function experiments, using complexes of antibodies and recombinant cytokines (cIL2), to dissect how T_{regs} exert their effects. Sex- and age-matched littermates were assigned randomly to groups. This study was not blinded. Each experiment was repeated at least two, usually three, times. Experimental and sample replicates as well as types of statistical analyses for each experiment are stated in the corresponding figure legends.

Mice

Foxp3$^{IRES\text{-}GFP}$ (termed B6.*Foxp3*^{Gfp} *here*) mice (*120*) were obtained from V. Kuchroo (Brigham and Women's Hospital, Boston, MA), while *Foxp3*^{DTR} *(termed B6.FoxP3*^{Dtr} *here)* mice (*46*) came from A. Rudensky (Memorial Sloan Kettering Cancer Center, NY, NY). 6wk- to 7wk-old male mice were used for all experiments unless otherwise specified. For RNA-seq experiments, 6wk- or 15wk-old male mice were used. Mice were housed in our specific-pathogen-free facility at Harvard Medical School (HMS). For the time course experiment, 3wk-, 52wk-, and 72wk-old C57BL/6J (B6) mice were purchased from the Jackson Laboratory and acclimated in our facility for at least 3 wks. Balb/cJ, NOD/ShiLtJ and C3H/HeJ mice were purchased at 3 wks of age from Jackson Laboratory and acclimated in our facility for at least 3 wks. All experiments were conducted under a protocol (#IS00001257) approved by HMS's Institutional Animal Care and Use Committee.

Mouse treatments

For all the experiments, mice were intracardially perfused with at least 35 mL of cold phosphate-buffered saline (PBS) before harvesting tissues. For T_{reg} ablation, B6.Foxp3Dtr+ mice and B6.Foxp3Dtr- littermates received 20 ng/g DT (Sigma) i.p. for 3 days. Intravascular immunocyte labeling followed established protocols (*52*): mice were anesthetized, injected intracardially with 25 μL (5 μg) anti-CD45 PE mAb (BioLegend), and blood collected 3 min later to confirm labeling. Mice were then perfused and tissues harvested.

For IFN-γ neutralization, mice received 250 μg i.p. anti-IFN-γ mAb (BioLegend, Ultra-LEAF purified XMG1.2) or IgG1κ isotype control every 48 hr, starting 8 hr before DT injection. For IL-2 neutralization, mice received 100 μg i.p. anti-IL-2 mAb (BioLegend Ultra-LEAF purified, JES6-1A12,) or IgG2aκ isotype control daily, starting 6 hr before DT injection. IL-2-anti-IL-2 complexes were prepared by incubating IL-2 (PeproTech) with anti-IL-2 antibodies JES6-1A12 (5 μg/0.5 μg) (*121*) or S4B6 (50 μg/5 μg; BD or BioXcell) (*97*), on ice for 30 min, resuspended in 100 μL PBS, and injected i.p. To block lymphocyte egress, mice received 1 mg/kg i.p. FTY720 (Cayman Chemical) 6 hr before DT injection and daily thereafter (*39*).

Intracisterna-magna injections

Injections into the cisterna magna were used to deliver 2.5 μg anti-CD25 mAb (BioLegend, Ultra-LEAF purified PC61) or an isotype control mAb (Biolegend, Ultra-LEAF purified rat IgG1λ) into the subarachnoid space in order to deplete meningeal T_{regs}. The procedure was performed as previously described (*50*).

Isolation of leukocytes from dura mater, leptomeninges, and choroid plexus dissection and digestion

All steps were performed on ice or cold blocks to preserve tissue quality. After perfusion, the bottom of the skull was removed to expose the brain parenchyma, and the brain was carefully extracted. Skullcaps with adhered meninges were stored in cold RPMI-1640 medium (Thermo Fisher) with 2% FBS until dissection. Dura mater was peeled from the skull under a dissecting microscope and digested in 2 mL RPMI with 2% FBS, 0.1 μg/mL DNAse I (Sigma), and 0.5 mg/mL collagenase P (Roche) at room temperature (RT) with shaking for 45 minutes. Digested samples were filtered through 100 μm strainers (Falcon) pre-wet with RPMI/FBS to reduce stickiness, using pre-coated pipette tips for disaggregation. Filters were washed twice with 15 mL RPMI/FBS, and cell suspensions were centrifuged at 520×g for 6 minutes. Pellets were resuspended in RPMI/FBS to the desired volume for downstream applications.

Skull bone marrow dissection

After meninges removal, skullcaps were placed in 1.5 mL Eppendorf tubes with 1 mL RPMI/FBS, finely chopped, and filtered through 70 μm strainers to remove bone fragments. The samples were washed with 10 mL RPMI/FBS, centrifuged at 520×g for 5 minutes, subjected to red blood cell lysis (Gibco), and washed again with 10 mL RPMI/FBS.

Spleen preparation

Immunocytes were isolated by mechanical disruption, followed by red blood cell lysis, filtration through a 40 μm strainer, and washing with 10 mL RPMI/FBS.

Brain dissection and digestion

Brains stored in cold HBSS (Gibco) were placed on ice to minimize cell death. Whole-brains (minus cerebellum) were minced with a blade on an ice-cold Petri dish, collected in HBSS, and centrifuged at 500×g for 5 minutes. After decanting the supernatant, 4 mL of pre-warmed digestion buffer (RPMI, 10 mM HEPES, 0.5 mg/mL Collagenase IV [Gibco], 0.6 mg/mL DNase I [Sigma]) was added, and samples were incubated at 37°C with constant agitation for 45 minutes. Samples were centrifuged (500×g, 5 minutes), the supernatant decanted, and the pellet resuspended in 2 mL cold FACS buffer (PBS, 2.5% FBS, 2 mM EDTA, 0.1% sodium azide). Tissue was triturated with a 1 mL pipette (20–30 times), filtered through a 70 μm strainer into a 15 mL Falcon tube, and mixed with 5 mL of 25% BSA. After centrifugation (1200×g, 10 minutes), the myelin layer was removed, the supernatant aspirated, and the pellet resuspended in FACS buffer for downstream analysis.

Regions of interest were dissected under a microscope, avoiding choroid plexus contamination, and placed in 2 mL microtubes (AXYGEN, ref MCT-200-C-S). Single-cell suspensions were prepared using the Miltenyi Neural Dissociation Kit (T) (ref 130-093-231) with modifications: manual mechanical dissociation replaced GentleMACS, followed by a 15-minute incubation at 37°C with slow rotation. Enzyme Mix 2 was added, and tubes were pipetted gently (15 times) in a 37°C water bath, repeating for 20 minutes. Samples were filtered and washed per the manufacturer's instructions.

Flow cytometry

The antibodies we used for flow cytometric staining (concentration 1:100, unless specified) are listed on table S1. Surface staining was performed for 30 minutes at 4°C, with viability assessed using Zombie UV Fixable Viability Dye (1:250), Zombie Yellow (1:1000), or Zombie NIR (1:1000) Fixable Viability Dye (BioLegend), following the manufacturer's instructions. For Annexin V, samples were washed twice with Annexin V binding buffer (BioLegend) and incubated with Annexin V alone for 15 minutes at RT. Intracellular staining used eBioscience's Foxp3/Transcription Factor Staining Buffer Set. For ex-vivo intracellular cytokine staining, single-cell suspensions were stimulated for 3.5 hours at 37°C with 50 ng/mL PMA and 1 mM ionomycin (Sigma-Aldrich), with protein transport inhibitor (eBioscience) in complete RPMI medium supplemented with 10% FBS. Cells were acquired on a FACSymphony flow cytometer (BD Biosciences) and analyzed using FlowJo software (Tree Star).

Statistical analyses

All statistical analyses were performed using GraphPad Prism software. If not stated otherwise, data are presented as mean ± SEM. Statistical significance was calculated by an unpaired Student's *t* test (two-tailed). For multiple comparisons involving two independent variables we used two-way ANOVA, and for multiple comparisons with one independent factor the statistical significance was calculated using a one-way ANOVA. For correlation between two factors simple linear regression analysis was performed. As indicated in the figure legend, $p < 0.05$ was considered significant. P-values for gene-signature enrichment or impoverishment between a pairwise comparison via volcano plots or FC/FC plots were determined using the χ^2 test. *$p <$ 0.05, **$p < 0.01$, ***$p < 0.001$, ****$p < 0.0001$. The statistical test used in each panel is described in the figure captions.

Supplementary Materials

The PDF file includes:
Materials and Methods
Figs. S1 to S12
Tables S1 to S3
References (*122–126*, *128–131*)

Other Supplementary Material for this manuscript includes the following:
Data files S1 to S4
MDAR Reproducibility Checklist

REFERENCES AND NOTES

1. R. Rua, D. B. McGavern, Advances in meningeal immunity. *Trends Mol. Med.* **24**, 542–559 (2018).
2. J. Rustenhoven, J. Kipnis, Brain borders at the central stage of neuroimmunology. *Nature* **612**, 417–429 (2022).
3. A. F. M. Salvador, N. Abduljawad, J. Kipnis, Meningeal lymphatics in central nervous system diseases. *Annu. Rev. Neurosci.* **47**, 323–344 (2024).
4. J. Kipnis, S. Gadani, N. C. Derecki, Pro-cognitive properties of T cells. *Nat. Rev. Immunol.* **12**, 663–669 (2012).
5. L. Rattazzi, G. Piras, M. Ono, R. Deacon, C. M. Pariante, F. D'Acquisto, $CD4^+$ but not $CD8^+$ T cells revert the impaired emotional behavior of immunocompromised RAG-1-deficient mice. *Transl. Psychiatry* **3**, e280 (2013).
6. J. Isung, K. Williams, K. Isomura, C. Gromark, E. Hesselmark, P. Lichtenstein, H. Larsson, L. Fernández de la Cruz, A. Sidorchuk, D. Mataix-Cols, Association of primary humoral immunodeficiencies with psychiatric disorders and suicidal behavior and the role of autoimmune diseases. *JAMA Psychiatry* **77**, 1147–1154 (2020).
7. O. R. Manusama, N. J. M. van Beveren, P. M. van Hagen, H. A. Drexhage, V. A. S. H. Dalm, Psychological symptoms in primary immunodeficiencies: A common comorbidity? *J. Clin. Immunol.* **42**, 695–698 (2022).
8. N. C. Derecki, A. N. Cardani, C. H. Yang, K. M. Quinnies, A. Crihfield, K. R. Lynch, J. Kipnis, Regulation of learning and memory by meningeal immunity: A key role for IL-4. *J. Exp. Med.* **207**, 1067–1080 (2010).
9. J. Herz, Z. Fu, K. Kim, T. Dykstra, M. Wall, H. Li, A. F. Salvador, B. Zou, N. Yan, S. M. Blackburn, P. H. Andrews, D. H. Goldman, Z. Papadopoulos, I. Smirnov, X. S. Xie, J. Kipnis, GABAergic neuronal IL-4R mediates T cell effect on memory. *Neuron* **109**, 3609–3618.e9 (2021).
10. M. D. Reed, Y. S. Yim, R. D. Wimmer, H. Kim, C. Ryu, G. M. Welch, M. Andina, H. O. King, A. Waisman, M. M. Halassa, J. R. Huh, G. B. Choi, IL-17a promotes sociability in mouse models of neurodevelopmental disorders. *Nature* **577**, 249–253 (2020).
11. A. J. Filiano, Y. Xu, N. J. Tustison, R. L. Marsh, W. Baker, I. Smirnov, C. C. Overall, S. P. Gadani, S. D. Turner, Z. Weng, S. N. Peerzade, H. Chen, K. S. Lee, M. M. Scott, M. P. Beenhakker, V. Litvak, J. Kipnis, Unexpected role of interferon-gamma in regulating neuronal connectivity and social behaviour. *Nature* **535**, 425–429 (2016).
12. B. W. Dulken, M. T. Buckley, P. Navarro Negredo, N. Saligrama, R. Cayrol, D. S. Leeman, B. M. George, S. C. Boutet, K. Hebestreit, J. V. Pluvinage, T. Wyss-Coray, I. L. Weissman, H. Vogel, M. M. Davis, A. Brunet, Single-cell analysis reveals T cell infiltration in old neurogenic niches. *Nature* **571**, 205–210 (2019).
13. S. Monteiro, F. M. Ferreira, V. Pinto, S. Roque, M. Morais, D. de Sá-Calçada, C. Mota, M. Correia-Neves, J. J. Cerqueira, Absence of IFNγ promotes hippocampal plasticity and enhances cognitive performance. *Transl. Psychiatry* **6**, e707 (2016).
14. S. Habbas, M. Santello, D. Becker, H. Stubbe, G. Zappia, N. Liaudet, F. R. Klaus, G. Kollias, A. Fontana, C. R. Pryce, T. Suter, A. Volterra, Neuroinflammatory TNFα impairs memory via astrocyte signaling. *Cell* **163**, 1730–1741 (2015).
15. Y. Zhang, J. T. Bailey, E. Xu, K. Singh, M. Lavaert, V. M. Link, S. D'Souza, A. Hafiz, J. Cao, G. Cao, D. B. Sant'Angelo, W. Sun, Y. Belkaid, A. Bhandoola, D. B. McGavern, Q. Yang, Mucosal-associated invariant T cells restrict reactive oxidative damage and preserve meningeal barrier integrity and cognitive function. *Nat. Immunol.* **23**, 1714–1725 (2022).
16. M. Ribeiro, H. C. Brigas, M. Temido-Ferreira, P. A. Pousinha, T. Regen, C. Santa, J. E. Coelho, I. Marques-Morgado, C. A. Valente, S. Omenetti, B. Stockinger, A. Waisman, B. Manadas, L. V. Lopes, B. Silva-Santos, J. C. Ribot, Meningeal γδ T cell-derived IL-17 controls synaptic plasticity and short-term memory. *Sci. Immunol.* **4**, eaay5199 (2019).
17. K. Alves de Lima, J. Rustenhoven, S. da Mesquita, M. Wall, A. F. Salvador, I. Smirnov, G. Martelossi Cebinelli, T. Mamuladze, W. Baker, Z. Papadopoulos, M. B. Lopes, W. S. Cao, X. S. Xie, J. Herz, J. Kipnis, Meningeal γδ T cells regulate anxiety-like behavior via IL-17a signaling in neurons. *Nat. Immunol.* **21**, 1421–1429 (2020).
18. S. Dikiy, A. Y. Rudensky, Principles of regulatory T cell function. *Immunity* **56**, 240–255 (2023).
19. A. R. Muñoz-Rojas, D. Mathis, Tissue regulatory T cells: Regulatory chameleons. *Nat. Rev. Immunol.* **21**, 597–611 (2021).
20. S. Da Mesquita, J. Herz, M. Wall, T. Dykstra, K. Alves de Lima, G. T. Norris, N. Dabhi, T. Kennedy, W. Baker, J. Kipnis, Aging-associated deficit in CCR7 is linked to worsened glymphatic function, cognition, neuroinflammation, and β-amyloid pathology. *Sci. Adv.* **7**, eabe4601 (2021).
21. M. J. C. Jordão, R. Sankowski, S. M. Brendecke, Sagar, G. Locatelli, Y. H. Tai, T. L. Tay, E. Schramm, S. Armbruster, N. Hagemeyer, O. Groß, D. Mai, Ö. Çiçek, T. Falk, M. Kerschensteiner, D. Grün, M. Prinz, Single-cell profiling identifies myeloid cell subsets with distinct fates during neuroinflammation. *Science* **363**, eaat7554 (2019).
22. M. Cabeza-Cabrerizo, A. Cardoso, C. M. Minutti, M. Pereira da Costa, C. Reis e Sousa, Dendritic cells revisited. *Annu. Rev. Immunol.* **39**, 131–166 (2021).
23. G. Garg, A. Muschaweckh, H. Moreno, A. Vasanthakumar, S. Floess, G. Lepennetier, R. Oellinger, Y. Zhan, T. Regen, M. Hiltensperger, C. Peter, L. Aly, B. Knier, L. R. Palam, R. Kapur, M. H. Kaplan, A. Waisman, R. Rad, G. Schotta, J. Huehn, A. Kallies, T. Korn, Blimp1 prevents methylation of Foxp3 and loss of regulatory T cell identity at sites of inflammation. *Cell Rep.* **26**, 1854–1868.e5 (2019).
24. J. Wang, L. Xie, C. Yang, C. Ren, K. Zhou, B. Wang, Z. Zhang, Y. Wang, K. Jin, G.-Y. Yang, Activated regulatory T cell regulates neural stem cell proliferation in the subventricular zone of normal and ischemic mouse brain through interleukin 10. *Front. Cell. Neurosci.* **9**, 361 (2015).
25. H. Taniguchi, I. Mohri, H. Okabe-Arahori, K. Aritake, K. Wada, T. Kanekiyo, S. Narumiya, M. Nakayama, K. Ozono, Y. Urade, M. Taniike, Prostaglandin D2 protects neonatal mouse brain from hypoxic ischemic injury. *J. Neurosci.* **27**, 4303–4312 (2007).
26. K. Maiese, WISP1: Clinical insights for a proliferative and restorative member of the CCN family. *Curr. Neurovasc. Res.* **11**, 378–389 (2014).
27. T. Katura, T. Moriya, N. Nakahata, 15-Deoxy-delta 12,14-prostaglandin J2 biphasically regulates the proliferation of mouse hippocampal neural progenitor cells by modulating the redox state. *Mol. Pharmacol.* **77**, 601–611 (2010).
28. R. M. Hoek, S. R. Ruuls, C. A. Murphy, G. J. Wright, R. Goddard, S. M. Zurawski, B. Blom, M. E. Homola, W. J. Streit, M. H. Brown, A. N. Barclay, J. D. Sedgwick, Down-regulation of the macrophage lineage through interaction with OX2 (CD200). *Science* **290**, 1768–1771 (2000).
29. M. De Saint Jean, F. Brignole, G. Feldmann, A. Goguel, C. Baudouin, Interferon-γ induces apoptosis and expression of inflammation-related proteins in Chang conjunctival cells. *Invest. Ophthalmol. Vis. Sci.* **40**, 2199–2212 (1999).
30. S. Takashima, M. L. Martin, S. A. Jansen, Y. Fu, J. Bos, D. Chandra, M. H. O'Connor, A. M. Mertelsmann, P. Vinci, J. Kuttiyara, S. M. Devlin, S. Middendorp, M. Calafiore,

A. Egorova, M. Kleppe, Y. Lo, N. F. Shroyer, E. H. Cheng, R. L. Levine, C. Liu, R. Kolesnick, C. A. Lindemans, A. M. Hanash, T cell–derived interferon-γ programs stem cell death in immune-mediated intestinal damage. *Sci. Immunol.* **4**, eaay8556 (2019).
31. F. Herisson, V. Frodermann, G. Courties, D. Rohde, Y. Sun, K. Vandoorne, G. R. Wojtkiewicz, G. S. Masson, C. Vinegoni, J. Kim, D. E. Kim, R. Weissleder, F. K. Swirski, M. A. Moskowitz, M. Nahrendorf, Direct vascular channels connect skull bone marrow and the brain surface enabling myeloid cell migration. *Nat. Neurosci.* **21**, 1209–1217 (2018).
32. A. Cugurra, T. Mamuladze, J. Rustenhoven, T. Dykstra, G. Beroshvili, Z. J. Greenberg, W. Baker, Z. Papadopoulos, A. Drieu, S. Blackburn, M. Kanamori, S. Brioschi, J. Herz, L. G. Schuettpelz, M. Colonna, I. Smirnov, J. Kipnis, Skull and vertebral bone marrow are myeloid cell reservoirs for the meninges and CNS parenchyma. *Science* **373**, eabf7844 (2021).
33. J. A. Mazzitelli, L. C. D. Smyth, K. A. Cross, T. Dykstra, J. Sun, S. du, T. Mamuladze, I. Smirnov, J. Rustenhoven, J. Kipnis, Cerebrospinal fluid regulates skull bone marrow niches via direct access through dural channels. *Nat. Neurosci.* **25**, 555–560 (2022).
34. J. Rustenhoven, A. Drieu, T. Mamuladze, K. A. de Lima, T. Dykstra, M. Wall, Z. Papadopoulos, M. Kanamori, A. F. Salvador, W. Baker, M. Lemieux, S. da Mesquita, A. Cugurra, J. Fitzpatrick, S. Sviben, R. Kossina, P. Bayguinov, R. R. Townsend, Q. Zhang, P. Erdmann-Gilmore, I. Smirnov, M. B. Lopes, J. Herz, J. Kipnis, Functional characterization of the dural sinuses as a neuroimmune interface. *Cell* **184**, 1000–1016.e27 (2021).
35. A. G. Levine, A. Mendoza, S. Hemmers, B. Moltedo, R. E. Niec, M. Schizas, B. E. Hoyos, E. V. Putintseva, A. Chaudhry, S. Dikiy, S. Fujisawa, D. M. Chudakov, P. M. Treuting, A. Y. Rudensky, Stability and function of regulatory T cells expressing the transcription factor T-bet. *Nature* **546**, 421–425 (2017).
36. M. A. Koch, G. Tucker-Heard, N. R. Perdue, J. R. Killebrew, K. B. Urdahl, D. J. Campbell, The transcription factor T-bet controls regulatory T cell homeostasis and function during type 1 inflammation. *Nat. Immunol.* **10**, 595–602 (2009).
37. P. Gonzalez-Figueroa, J. A. Roco, I. Papa, L. Núñez Villacís, M. Stanley, M. A. Linterman, A. Dent, P. F. Canete, C. G. Vinuesa, Follicular regulatory T cells produce neuritin to regulate B cells. *Cell* **184**, 1775–1789.e19 (2021).
38. P. T. Sage, A. H. Sharpe, The multifaceted functions of follicular regulatory T cells. *Curr. Opin. Immunol.* **67**, 68–74 (2020).
39. B. S. Hanna, G. Wang, S. Galván-Peña, A. O. Mann, R. N. Ramirez, A. R. Muñoz-Rojas, K. Smith, M. Wan, C. Benoist, D. Mathis, The gut microbiota promotes distal tissue regeneration via RORγ$^+$ regulatory T cell emissaries. *Immunity* **56**, 829–846.e8 (2023).
40. T. Xiao, P. K. Langston, A. R. Muñoz-Rojas, T. Jayewickreme, M. A. Lazar, C. Benoist, D. Mathis, T_{regs} in visceral adipose tissue up-regulate circadian-clock expression to promote fitness and enforce a diurnal rhythm of lipolysis. *Sci. Immunol.* **7**, eabl7641 (2022).
41. T. G. Tan, D. Mathis, C. Benoist, Singular role for T-BET$^+$CXCR3$^+$ regulatory T cells in protection from autoimmune diabetes. *Proc. Natl. Acad. Sci. U.S.A.* **113**, 14103–14108 (2016).
42. W. Sungnak, A. Wagner, M. S. Kowalczyk, L. Bod, Y. C. Kye, P. T. Sage, A. H. Sharpe, R. A. Sobel, F. J. Quintana, O. Rozenblatt-Rosen, A. Regev, C. Wang, N. Yosef, V. K. Kuchroo, T follicular regulatory cell-derived fibrinogen-like protein 2 regulates production of autoantibodies and induction of systemic autoimmunity. *J. Immunol.* **205**, 3247–3262 (2020).
43. S. Suvas, A. K. Azkur, B. S. Kim, U. Kumaraguru, B. T. Rouse, CD4+CD25+ regulatory T cells control the severity of viral immunoinflammatory lesions. *J. Immunol.* **172**, 4123–4132 (2004).
44. D. Burzyn, W. Kuswanto, D. Kolodin, J. L. Shadrach, M. Cerletti, Y. Jang, E. Sefik, T. G. Tan, A. J. Wagers, C. Benoist, D. Mathis, A special population of regulatory T cells potentiates muscle repair. *Cell* **155**, 1282–1295 (2013).
45. Y. Y. Setiady, J. A. Coccia, P. U. Park, In vivo depletion of CD4+FOXP3+ Treg cells by the PC61 anti-CD25 monoclonal antibody is mediated by FcgammaRIII+ phagocytes. *Eur. J. Immunol.* **40**, 780–786 (2010).
46. J. M. Kim, J. P. Rasmussen, A. Y. Rudensky, Regulatory T cells prevent catastrophic autoimmunity throughout the lifespan of mice. *Nat. Immunol.* **8**, 191–197 (2007).
47. A. Drieu, S. Du, S. E. Storck, J. Rustenhoven, Z. Papadopoulos, T. Dykstra, F. Zhong, K. Kim, S. Blackburn, T. Mamuladze, O. Harari, C. M. Karch, R. J. Bateman, R. Perrin, M. Farlow, J. Chhatwal, Dominantly Inherited Alzheimer Network, S. Hu, G. J. Randolph, I. Smirnov, J. Kipnis, Parenchymal border macrophages regulate the flow dynamics of the cerebrospinal fluid. *Nature* **611**, 585–593 (2022).
48. Y. Wang, D. Chen, D. Xu, C. Huang, R. Xing, D. He, H. Xu, Early developing B cells undergo negative selection by central nervous system-specific antigens in the meninges. *Immunity* **54**, 2784–2794.e6 (2021).
49. S. Brioschi, W. L. Wang, V. Peng, M. Wang, I. Shchukina, Z. J. Greenberg, J. K. Bando, N. Jaeger, R. S. Czepielewski, A. Swain, D. A. Mogilenko, W. L. Beatty, P. Bayguinov, J. A. J. Fitzpatrick, L. G. Schuettpelz, C. C. Fronick, I. Smirnov, J. Kipnis, V. S. Shapiro, G. F. Wu, S. Gilfillan, M. Cella, M. N. Artyomov, S. H. Kleinstein, M. Colonna, Heterogeneity of meningeal B cells reveals a lymphopoietic niche at the CNS borders. *Science* **373**, eabf9277 (2021).
50. F. A. Pinho-Ribeiro, L. Deng, D. V. Neel, O. Erdogan, H. Basu, D. Yang, S. Choi, A. J. Walker, S. Carneiro-Nascimento, K. He, G. Wu, B. Stevens, K. S. Doran, D. Levy, I. M. Chiu, Bacteria hijack a meningeal neuroimmune axis to facilitate brain invasion. *Nature* **615**, 472–481 (2023).
51. Z. Fitzpatrick, G. Frazer, A. Ferro, S. Clare, N. Bouladoux, J. Ferdinand, Z. K. Tuong, M. L. Negro-Demontel, N. Kumar, O. Suchanek, T. Tajsic, K. Harcourt, K. Scott, R. Bashford-Rogers, A. Helmy, D. S. Reich, Y. Belkaid, T. D. Lawley, D. B. McGavern, M. R. Clatworthy, Gut-educated IgA plasma cells defend the meningeal venous sinuses. *Nature* **587**, 472–476 (2020).
52. K. G. Anderson, K. Mayer-Barber, H. Sung, L. Beura, B. R. James, J. J. Taylor, L. Qunaj, T. S. Griffith, V. Vezys, D. L. Barber, D. Masopust, Intravascular staining for discrimination of vascular and tissue leukocytes. *Nat. Protoc.* **9**, 209–222 (2014).
53. J. I. Morgan, D. R. Cohen, J. L. Hempstead, T. Curran, Mapping patterns of c-fos expression in the central nervous system after seizure. *Science* **237**, 192–197 (1987).
54. J. L. Zamanian, L. Xu, L. C. Foo, N. Nouri, L. Zhou, R. G. Giffard, B. A. Barres, Genomic analysis of reactive astrogliosis. *J. Neurosci.* **32**, 6391–6410 (2012).
55. H. Keren-Shaul, A. Spinrad, A. Weiner, O. Matcovitch-Natan, R. Dvir-Szternfeld, T. K. Ulland, E. David, K. Baruch, D. Lara-Astaiso, B. Toth, S. Itzkovitz, M. Colonna, M. Schwartz, I. Amit, A unique microglia type associated with restricting development of Alzheimer's disease. *Cell* **169**, 1276–1290.e17 (2017).
56. T. R. Hammond, C. Dufort, L. Dissing-Olesen, S. Giera, A. Young, A. Wysoker, A. J. Walker, F. Gergits, M. Segel, J. Nemesh, S. E. Marsh, A. Saunders, E. Macosko, F. Ginhoux, J. Chen, R. J. M. Franklin, X. Piao, S. A. McCarroll, B. Stevens, Single-cell RNA sequencing of microglia throughout the mouse lifespan and in the injured brain reveals complex cell-state changes. *Immunity* **50**, 253–271.e6 (2019).
57. M. A. Wheeler, I. C. Clark, E. C. Tjon, Z. Li, S. E. J. Zandee, C. P. Couturier, B. R. Watson, G. Scalisi, S. Alkwai, V. Rothhammer, A. Rotem, J. A. Heyman, S. Thaploo, L. M. Sanmarco, J. Ragoussis, D. A. Weitz, K. Petrecca, J. R. Moffitt, B. Becher, J. P. Antel, A. Prat, F. J. Quintana, MAFG-driven astrocytes promote CNS inflammation. *Nature* **578**, 593–599 (2020).
58. C. Schmitt, N. Strazielle, J. F. Ghersi-Egea, Brain leukocyte infiltration initiated by peripheral inflammation or experimental autoimmune encephalomyelitis occurs through pathways connected to the CSF-filled compartments of the forebrain and midbrain. *J. Neuroinflammation* **9**, 187 (2012).
59. L. Cicchini, J. A. Westrich, T. Xu, D. W. Vermeer, J. N. Berger, E. T. Clambey, D. Lee, J. I. Song, P. F. Lambert, R. O. Greer, J. H. Lee, D. Pyeon, Suppression of antitumor immune responses by human papillomavirus through epigenetic downregulation of CXCL14. *mBio* **7**, e00270-16 (2016).
60. J. A. Westrich, D. W. Vermeer, A. Silva, S. Bonney, J. N. Berger, L. Cicchini, R. O. Greer, J. I. Song, D. Raben, J. E. Slansky, J. H. Lee, W. C. Spanos, D. Pyeon, CXCL14 suppresses human papillomavirus-associated head and neck cancer through antigen-specific CD8$^+$ T-cell responses by upregulating MHC-I expression. *Oncogene* **38**, 7166–7180 (2019).
61. H.-T. Lee, S.-P. Liu, C.-H. Lin, S. W. Lee, C. Y. Hsu, H.-K. Sytwu, C.-H. Hsieh, W.-C. Shyu, A crucial role of CXCL14 for promoting regulatory T cells activation in stroke. *Theranostics* **7**, 855–875 (2017).
62. N. J. Allen, D. A. Lyons, Glia as architects of central nervous system formation and function. *Science* **362**, 181–185 (2018).
63. B. Asrican, J. Wooten, Y. D. Li, L. Quintanilla, F. Zhang, C. Wander, H. Bao, C.-Y. Yeh, Y.-J. Luo, R. Olsen, S.-A. Lim, J. Hu, P. Jin, J. Song, Neuropeptides modulate local astrocytes to regulate adult hippocampal neural stem cells. *Neuron* **108**, 349–366.e6 (2020).
64. A. Adamsky, A. Kol, T. Kreisel, A. Doron, N. Ozeri-Engelhard, T. Melcer, R. Refaeli, H. Horn, L. Regev, M. Groysman, M. London, I. Goshen, Astrocytic activation generates de novo neuronal potentiation and memory enhancement. *Cell* **174**, 59–71.e14 (2018).
65. A. Doron, A. Rubin, A. Benmelech-Chovav, N. Benaim, T. Carmi, R. Refaeli, N. Novick, T. Kreisel, Y. Ziv, I. Goshen, Hippocampal astrocytes encode reward location. *Nature* **609**, 772–778 (2022).
66. P. Kofuji, A. Araque, Astrocytes and behavior. *Annu. Rev. Neurosci.* **44**, 49–67 (2021).
67. F. Provenzano, M. J. Perez, M. Deleidi, Redefining microglial identity in health and disease at single-cell resolution. *Trends Mol. Med.* **27**, 47–59 (2021).
68. A. Bonafina, G. Paratcha, F. Ledda, Deciphering new players in the neurogenic adult hippocampal niche. *Front. Cell Dev. Biol.* **8**, 548 (2020).
69. J. Karpf, P. Unichenko, N. Chalmers, F. Beyer, M. T. Wittmann, J. Schneider, E. Fidan, A. Reis, J. Beckervordersandforth, S. Brandner, S. Liebner, S. Falk, A. Sagner, C. Henneberger, R. Beckervordersandforth, Dentate gyrus astrocytes exhibit layer-specific molecular, morphological and physiological features. *Nat. Neurosci.* **25**, 1626–1638 (2022).
70. H. Hochgerner, A. Zeisel, P. Lonnerberg, S. Linnarsson, Conserved properties of dentate gyrus neurogenesis across postnatal development revealed by single-cell RNA sequencing. *Nat. Neurosci.* **21**, 290–299 (2018).
71. R. M. Beiter, C. Rivet-Noor, A. R. Merchak, R. Bai, D. M. Johanson, E. Slogar, K. Sol-Church, C. C. Overall, A. Gaultier, Evidence for oligodendrocyte progenitor cell heterogeneity in the adult mouse brain. *Sci. Rep.* **12**, 12921 (2022).

72. A. Denoth-Lippuner, S. Jessberger, Formation and integration of new neurons in the adult hippocampus. *Nat. Rev. Neurosci.* **22**, 223–236 (2021).
73. J. Terreros-Roncal, E. P. Moreno-Jiménez, M. Flor-García, C. B. Rodríguez-Moreno, M. F. Trinchero, F. Cafini, A. Rábano, M. Llorens-Martín, Impact of neurodegenerative diseases on human adult hippocampal neurogenesis. *Science* **374**, 1106–1113 (2021).
74. J. T. Goncalves, S. T. Schafer, F. H. Gage, Adult Neurogenesis in the hippocampus: From stem cells to behavior. *Cell* **167**, 897–914 (2016).
75. W. Deng, J. B. Aimone, F. H. Gage, New neurons and new memories: How does adult hippocampal neurogenesis affect learning and memory? *Nat. Rev. Neurosci.* **11**, 339–350 (2010).
76. R. T. Káradóttir, C. T. Kuo, Neuronal activity-dependent control of postnatal neurogenesis and gliogenesis. *Annu. Rev. Neurosci.* **41**, 139–161 (2018).
77. K. loi Vong, C. K. Leung, R. R. Behringer, K. M. Kwan, Sox9 is critical for suppression of neurogenesis but not initiation of gliogenesis in the cerebellum. *Mol. Brain* **8**, 25 (2015).
78. R. Sueda, I. Imayoshi, Y. Harima, R. Kageyama, High Hes1 expression and resultant Ascl1 suppression regulate quiescent vs. active neural stem cells in the adult mouse brain. *Genes Dev.* **33**, 511–523 (2019).
79. Z. Gao, K. Ure, J. L. Ables, D. C. Lagace, K. A. Nave, S. Goebbels, A. J. Eisch, J. Hsieh, Neurod1 is essential for the survival and maturation of adult-born neurons. *Nat. Neurosci.* **12**, 1090–1092 (2009).
80. S. Garza-Manero, A. A. A. Sindi, G. Mohan, O. Rehbini, V. H. M. Jeantet, M. Bailo, F. A. Latif, M. P. West, R. Gurden, L. Finlayson, S. Svambaryte, A. G. West, K. L. West, Maintenance of active chromatin states by HMGN2 is required for stem cell identity in a pluripotent stem cell model. *Epigenetics Chromatin* **12**, 73 (2019).
81. A. Zuccotti, C. le Magueresse, M. Chen, A. Neitz, H. Monyer, The transcription factor Fezf2 directs the differentiation of neural stem cells in the subventricular zone toward a cortical phenotype. *Proc. Natl. Acad. Sci. U.S.A.* **111**, 10726–10731 (2014).
82. P. Codega, V. Silva-Vargas, A. Paul, A. R. Maldonado-Soto, A. M. DeLeo, E. Pastrana, F. Doetsch, Prospective identification and purification of quiescent adult neural stem cells from their in vivo niche. *Neuron* **82**, 545–559 (2014).
83. N. Urban, I. M. Blomfield, F. Guillemot, Quiescence of adult mammalian neural stem cells: A highly regulated rest. *Neuron* **104**, 834–848 (2019).
84. M. Khacho, R. Harris, R. S. Slack, Mitochondria as central regulators of neural stem cell fate and cognitive function. *Nat. Rev. Neurosci.* **20**, 34–48 (2019).
85. E. Llorens-Bobadilla, S. Zhao, A. Baser, G. Saiz-Castro, K. Zwadlo, A. Martin-Villalba, Single-cell transcriptomics reveals a population of dormant neural stem cells that become activated upon brain injury. *Cell Stem Cell* **17**, 329–340 (2015).
86. M. A. Bonaguidi, M. A. Wheeler, J. S. Shapiro, R. P. Stadel, G. J. Sun, G. L. Ming, H. Song, In vivo clonal analysis reveals self-renewing and multipotent adult neural stem cell characteristics. *Cell* **145**, 1142–1155 (2011).
87. D. D. Liu, J. Q. He, R. Sinha, A. E. Eastman, A. M. Toland, M. Morri, N. F. Neff, H. Vogel, N. Uchida, I. L. Weissman, Purification and characterization of human neural stem and progenitor cells. *Cell* **186**, 1179–1194.e15 (2023).
88. D. A. Lim, A. Alvarez-Buylla, The adult ventricular–subventricular Zone (V-SVZ) and olfactory bulb (OB) neurogenesis. *Cold Spring Harb. Perspect. Biol.* **8**, a018820 (2016).
89. J. Walter, S. D. Honsek, S. Illes, J. M. Wellen, H. P. Hartung, C. R. Rose, M. Dihné, A new role for interferon gamma in neural stem/precursor cell dysregulation. *Mol. Neurodegener.* **6**, 18 (2011).
90. L. Li, T. L. Walker, Y. Zhang, E. W. Mackay, P. F. Bartlett, Endogenous interferon γ directly regulates neural precursors in the non-inflammatory brain. *J. Neurosci.* **30**, 9038–9050 (2010).
91. N. D. Leipzig, C. Xu, T. Zahir, M. S. Shoichet, Functional immobilization of interferon-gamma induces neuronal differentiation of neural stem cells. *J. Biomed. Mater. Res. A* **93**, 625–633 (2010).
92. R. Baron, A. Nemirovsky, I. Harpaz, H. Cohen, T. Owens, A. Monsonego, IFN-γ enhances neurogenesis in wild-type mice and in a mouse model of Alzheimer's disease. *FASEB J.* **22**, 2843–2852 (2008).
93. G. Wong, Y. Goldshmit, A. M. Turnley, Interferon-γ but not TNFα promotes neuronal differentiation and neurite outgrowth of murine adult neural stem cells. *Exp. Neurol.* **187**, 171–177 (2004).
94. K. Warre-Cornish, L. Perfect, R. Nagy, R. R. R. Duarte, M. J. Reid, P. Raval, A. Mueller, A. L. Evans, A. Couch, C. Ghevaert, G. McAlonan, E. Loth, D. Murphy, T. R. Powell, A. C. Vernon, D. P. Srivastava, J. Price, Interferon-γ signaling in human iPSC-derived neurons recapitulates neurodevelopmental disorder phenotypes. *Sci. Adv.* **6**, eaay9506 (2020).
95. B. A. Reynolds, S. Weiss, Generation of neurons and astrocytes from isolated cells of the adult mammalian central nervous system. *Science* **255**, 1707–1710 (1992).
96. R. Soares, F. F. Ribeiro, D. M. Lourenço, R. S. Rodrigues, J. B. Moreira, A. M. Sebastião, V. A. Morais, S. Xapelli, Isolation and expansion of neurospheres from postnatal (P1–3) mouse neurogenic niches. *J. Vis. Exp.* e60822 (2020).
97. J. Sitrin, A. Ring, K. C. Garcia, C. Benoist, D. Mathis, Regulatory T cells control NK cells in an insulitic lesion by depriving them of IL-2. *J. Exp. Med.* **210**, 1153–1165 (2013).
98. O. Boyman, J. Sprent, The role of interleukin-2 during homeostasis and activation of the immune system. *Nat. Rev. Immunol.* **12**, 180–190 (2012).
99. T. K. Yu, E. G. Caudell, C. Smid, E. A. Grimm, IL-2 activation of NK cells: Involvement of MKK1/2/ERK but not p38 kinase pathway. *J. Immunol.* **164**, 6244–6251 (2000).
100. S. L. McQuaid, S. T. Loughran, P. A. Power, P. Maguire, A. Szczygiel, P. A. Johnson, Low-dose IL-2 induces CD56^{bright} NK regulation of T cells via NKp44 and NKp46. *Clin. Exp. Immunol.* **200**, 228–241 (2020).
101. J. B. Spangler, J. Tomala, V. C. Luca, K. M. Jude, S. Dong, A. M. Ring, P. Votavova, M. Pepper, M. Kovar, K. C. Garcia, Antibodies to interleukin-2 elicit selective T cell subset potentiation through distinct conformational mechanisms. *Immunity* **42**, 815–825 (2015).
102. G. Castellani, T. Croese, J. M. Peralta Ramos, M. Schwartz, Transforming the understanding of brain immunity. *Science* **380**, eabo7649 (2023).
103. E. F. Willis, K. P. A. MacDonald, Q. H. Nguyen, A. L. Garrido, E. R. Gillespie, S. B. R. Harley, P. F. Bartlett, W. A. Schroder, A. G. Yates, D. C. Anthony, S. Rose-John, M. J. Ruitenberg, J. Vukovic, Repopulating microglia promote brain repair in an IL-6-dependent manner. *Cell* **180**, 833–846.e16 (2020).
104. S. A. Liddelow, K. A. Guttenplan, L. E. Clarke, F. C. Bennett, C. J. Bohlen, L. Schirmer, M. L. Bennett, A. E. Münch, W. S. Chung, T. C. Peterson, D. K. Wilton, A. Frouin, B. A. Napier, N. Panicker, M. Kumar, M. S. Buckwalter, D. H. Rowitch, V. L. Dawson, T. M. Dawson, B. Stevens, B. A. Barres, Neurotoxic reactive astrocytes are induced by activated microglia. *Nature* **541**, 481–487 (2017).
105. C. S. McAlpine, J. Park, A. Griciuc, E. Kim, S. H. Choi, Y. Iwamoto, M. G. Kiss, K. A. Christie, C. Vinegoni, W. C. Poller, J. E. Mindur, C. T. Chan, S. He, H. Janssen, L. P. Wong, J. Downey, S. Singh, A. Anzai, F. Kahles, M. Jorfi, P. F. Feruglio, R. I. Sadreyev, R. Weissleder, B. P. Kleinstiver, M. Nahrendorf, R. E. Tanzi, F. K. Swirski, Astrocytic interleukin-3 programs microglia and limits Alzheimer's disease. *Nature* **595**, 701–706 (2021).
106. F. Cassé, K. Richetin, N. Toni, Astrocytes' contribution to adult neurogenesis in physiology and Alzheimer's disease. *Front. Cell. Neurosci.* **12**, 432 (2018).
107. I. Diaz-Aparicio, I. Paris, V. Sierra-Torre, A. Plaza-Zabala, N. Rodríguez-Iglesias, M. Márquez-Ropero, S. Beccari, P. Huguet, O. Abiega, E. Alberdi, C. Matute, I. Bernales, A. Schulz, L. Otrokocsi, B. Sperlagh, K. E. Happonen, G. Lemke, M. Maletic-Savatic, J. Valero, A. Sierra, Microglia actively remodel adult hippocampal neurogenesis through the phagocytosis secretome. *J. Neurosci.* **40**, 1453–1482 (2020).
108. A. Sierra, J. M. Encinas, J. J. P. Deudero, J. H. Chancey, G. Enikolopov, L. S. Overstreet-Wadiche, S. E. Tsirka, M. Maletic-Savatic, Microglia shape adult hippocampal neurogenesis through apoptosis-coupled phagocytosis. *Cell Stem Cell* **7**, 483–495 (2010).
109. F. L'Episcopo, C. Tirolo, N. Testa, S. Caniglia, M. C. Morale, M. Deleidi, M. F. Serapide, S. Pluchino, B. Marchetti, Plasticity of subventricular zone neuroprogenitors in MPTP (1-methyl-4-phenyl-1,2,3,6-tetrahydropyridine) mouse model of Parkinson's disease involves cross talk between inflammatory and Wnt/β-catenin signaling pathways: Functional consequences for neuroprotection and repair. *J. Neurosci.* **32**, 2062–2085 (2012).
110. B. A. Benayoun, E. A. Pollina, P. P. Singh, S. Mahmoudi, I. Harel, K. M. Casey, B. W. Dulken, A. Kundaje, A. Brunet, Remodeling of epigenome and transcriptome landscapes with aging in mice reveals widespread induction of inflammatory responses. *Genome Res.* **29**, 697–709 (2019).
111. W. N. Jin, K. Shi, W. He, J. H. Sun, L. van Kaer, F. D. Shi, Q. Liu, Neuroblast senescence in the aged brain augments natural killer cell cytotoxicity leading to impaired neurogenesis and cognition. *Nat. Neurosci.* **24**, 61–73 (2021).
112. T. Kaya, N. Mattugini, L. Liu, H. Ji, L. Cantuti-Castelvetri, J. Wu, M. Schifferer, J. Groh, R. Martini, S. Besson-Girard, S. Kaji, A. Liesz, O. Gokce, M. Simons, CD8$^+$ T cells induce interferon-responsive oligodendrocytes and microglia in white matter aging. *Nat. Neurosci.* **25**, 1446–1457 (2022).
113. J. Groh, K. Knöpper, P. Arampatzi, X. Yuan, L. Lößlein, A.-E. Saliba, W. Kastenmüller, R. Martini, Accumulation of cytotoxic T cells in the aged CNS leads to axon degeneration and contributes to cognitive and motor decline. *Nat. Aging.* **1**, 357–367 (2021).
114. G. P. Williams, A. M. Schonhoff, A. Jurkuvenaite, N. J. Gallups, D. G. Standaert, A. S. Harms, CD4 T cells mediate brain inflammation and neurodegeneration in a mouse model of Parkinson's disease. *Brain* **144**, 2047–2059 (2021).
115. D. Gate, E. Tapp, O. Leventhal, M. Shahid, T. J. Nonninger, A. C. Yang, K. Strempfl, M. S. Unger, T. Fehlmann, H. Oh, D. Channappa, V. W. Henderson, A. Keller, L. Aigner, D. R. Galasko, M. M. Davis, K. L. Poston, T. Wyss-Coray, CD4$^+$ T cells contribute to neurodegeneration in Lewy body dementia. *Science* **374**, 868–874 (2021).
116. X. Chen, M. Firulyova, M. Manis, J. Herz, I. Smirnov, E. Aladyeva, C. Wang, X. Bao, M. B. Finn, H. Hu, I. Shchukina, M. W. Kim, C. M. Yuede, J. Kipnis, M. N. Artyomov, J. D. Ulrich, D. M. Holtzman, Microglia-mediated T cell infiltration drives neurodegeneration in tauopathy. *Nature* **615**, 668–677 (2023).
117. J. Machhi, P. Yeapuri, Y. Lu, E. Foster, R. Chikhale, J. Herskovitz, K. L. Namminga, K. E. Olson, M. M. Abdelmoaty, J. Gao, R. M. Quadros, T. Kiyota, L. Jingjing, B. D. Kevadiya, X. Wang, Y. Liu, L. Y. Poluektova, C. B. Gurumurthy, R. L. Mosley, H. E. Gendelman, CD4$^+$ effector T cells accelerate Alzheimer's disease in mice. *J. Neuroinflammation* **18**, 272 (2021).

118. C. Laurent, G. Dorothée, S. Hunot, E. Martin, Y. Monnet, M. Duchamp, Y. Dong, F. P. Légeron, A. Leboucher, S. Burnouf, E. Faivre, K. Carvalho, R. Caillierez, N. Zommer, D. Demeyer, N. Jouy, V. Sazdovitch, S. Schraen-Maschke, C. Delarasse, L. Buée, D. Blum, Hippocampal T cell infiltration promotes neuroinflammation and cognitive decline in a mouse model of tauopathy. *Brain* **140**, 184–200 (2017).
119. N. Piehl, L. van Olst, A. Ramakrishnan, V. Teregulova, B. Simonton, Z. Zhang, E. Tapp, D. Channappa, H. Oh, P. M. Losada, J. Rutledge, A. N. Trelle, E. C. Mormino, F. Elahi, D. R. Galasko, V. W. Henderson, A. D. Wagner, T. Wyss-Coray, D. Gate, Cerebrospinal fluid immune dysregulation during healthy brain aging and cognitive impairment. *Cell* **185**, 5028–5039.e13 (2022).
120. E. Bettelli, Y. Carrier, W. Gao, T. Korn, T. B. Strom, M. Oukka, H. L. Weiner, V. K. Kuchroo, Reciprocal developmental pathways for the generation of pathogenic effector TH17 and regulatory T cells. *Nature* **441**, 235–238 (2006).
121. M. Feuerer, L. Herrero, D. Cipolletta, A. Naaz, J. Wong, A. Nayer, J. Lee, A. B. Goldfine, C. Benoist, S. Shoelson, D. Mathis, Lean, but not obese, fat is enriched for a unique population of regulatory T cells that affect metabolic parameters. *Nat. Med.* **15**, 930–939 (2009).
122. Y. Zhang, W. Hu, Mouse enteric neuronal cell culture. *Methods Mol. Biol.* **1078**, 55–63 (2013).
123. P. K. Langston, Y. Sun, B. A. Ryback, A. L. Mueller, B. M. Spiegelman, C. Benoist, D. Mathis, Regulatory T cells shield muscle mitochondria from interferon-γ-mediated damage to promote the beneficial effects of exercise. *Sci Immunol.* **8**, eadi5377 (2023).
124. L. C. D. Smyth, D. Xu, S. V. Okar, T. Dykstra, J. Rustenhoven, Z. Papadopoulos, K. Bhasiin, M. W. Kim, A. Drieu, T. Mamuladze, S. Blackburn, X. Gu, M. I. Gaitán, G. Nair, S. E. Storck, S. du, M. A. White, P. Bayguinov, I. Smirnov, K. Dikranian, D. S. Reich, J. Kipnis, Identification of direct connections between the dura and the brain. *Nature* **627**, 165–173 (2024).
125. V. Bergen, M. Lange, S. Peidli, F. A. Wolf, F. J. Theis, Generalizing RNA velocity to transient cell states through dynamical modeling. *Nat. Biotechnol.* **38**, 1408–1414 (2020).
126. F. A. Wolf, F. K. Hamey, M. Plass, J. Solana, J. S. Dahlin, B. Göttgens, N. Rajewsky, L. Simon, F. J. Theis, PAGA: Graph abstraction reconciles clustering with trajectory inference through a topology preserving map of single cells. *Genome Biol.* **20**, 59 (2019).
127. Y. Zhou, B. Zhou, L. Pache, M. Chang, A. H. Khodabakhshi, O. Tanaseichuk, C. Benner, S. K. Chanda, Metascape provides a biologist-oriented resource for the analysis of systems-level datasets. *Nat. Commun.* **10**, 1523 (2019).
128. M. Delacher, C. D. Imbusch, D. Weichenhan, A. Breiling, A. Hotz-Wagenblatt, U. Träger, A. C. Hofer, D. Kägebein, Q. Wang, F. Frauhammer, J. P. Mallm, K. Bauer, C. Herrmann, P. A. Lang, B. Brors, C. Plass, M. Feuerer, Genome-wide DNA-methylation landscape defines specialization of regulatory T cells in tissues. *Nat. Immunol.* **18**, 1160–1172 (2017).
129. J. Cho, W. Kuswanto, C. Benoist, D. Mathis, T cell receptor specificity drives accumulation of a reparative population of regulatory T cells within acutely injured skeletal muscle. *Proc. Natl. Acad. Sci. U.S.A.* **116**, 26727–26733 (2019).
130. C. Neumann, J. Blume, U. Roy, P. P. Teh, A. Vasanthakumar, A. Beller, Y. Liao, F. Heinrich, T. L. Arenzana, J. A. Hackney, C. Eidenschenk, E. J. C. Gálvez, C. Stehle, G. A. Heinz, P. Maschmeyer, T. Sidwell, Y. Hu, D. Amsen, C. Romagnani, H. D. Chang, A. Kruglov, M. F. Mashreghi, W. Shi, T. Strowig, S. Rutz, A. Kallies, A. Scheffold, c-Maf-dependent Treg cell control of intestinal TH17 cells and IgA establishes host-microbiota homeostasis. *Nat. Immunol.* **20**, 471–481 (2019).
131. M. Marzec, K. Halasa, M. Kasprzycka, M. Wysocka, X. Liu, J. W. Tobias, D. Baldwin, Q. Zhang, N. Odum, A. H. Rook, M. A. Wasik, Differential effects of interleukin-2 and interleukin-15 versus interleukin-21 on CD4+ cutaneous T-cell lymphoma cells. *Cancer Res.* **68**, 1083–1091 (2008).

Acknowledgments: We gratefully acknowledge: M.R. Kasal for manuscript editing; B. Hanna, A. Muñoz-Rojas, V. Piekarsa, T. M. Fisher, K. Hattori and A. Ortiz-Lopez for experimental help and discussions; P.V. Anekal and the HMS MiCRoN Core for help with image acquisition and analyses; J. Lee, I. Magill, and the Broad Genomics Platform for RNA-seq; L. Yang and B. Vijaykumar for computational help; C. Laplace for graphics; B. Caldarone and the HMS Mouse Behavior Core; and the HMS Immunology Flow Cytometry Core. **Funding:** This work was funded by a grant from the JPB Foundation to D.M., by project grant P1D2019-110292RB-100 from the Spanish Ministry of Science and Innovation to J.L.T., by NIH grants R01AI168005 and R01DK127257 to I.M.C., and by an NIH Director's New Innovator Award (DP2-AI169979-01) and an award from the Crohn's & Colitis Foundation(#959859) to R.J. B.S. was funded through HHMI and Cure Alzheimer's Fund. E.C.R. was supported by a predoctoral fellowship (FPI) BES-2017/080415 from the Ministerio de Economia y Competitividad. **Author contributions:** MMR and DM conceptualized the study. MMR, ECR, AJW, TJ, FAPR and QR performed experiments and analyzed data. RJ, IMC, BS, JLT and DM provided funding. RJ, IMC, BS, JLT, CB and DM provided supervision. MMR and DM drafted the manuscript, which all authors reviewed. **Competing interests:** The authors declare no competing interests. **Data and materials availability:** New data generated for this report have been deposited in the Gene Expression Omnibus (GEO) database under the accession number GSE234317. Tabulated data underlying the figures is provided in data file S2. All other data needed to support the conclusions of the paper are present in the paper or the Supplementary Materials.

Submitted 31 October 2024
Accepted 22 January 2025
Published First Release 28 January 2025
10.1126/sciimmunol.adu2910

Abstract

One-sentence summary: Meningeal regulatory T cells restrain local interferon-γ–producing lymphocytes, thereby safeguarding parenchymal brain homeostasis.